Theory of two- and three-dimensional bent-core mesophases

B. Mettout
GCL, 33 rue St Leu, 80000 Amiens, France

(Received 31 March 2006; revised manuscript received 18 July 2006; published 19 January 2007)

An extension of the vector-wave theory of antiferroelectric bent-core liquid crystals to columnar and soft-crystalline mesophases is presented. We enumerate and describe the phases resulting from the condensation of one, two, and three vector waves in the isotropic liquid of bent-core molecules. Beside the one-dimensional $B2$ and smectic-CP phases, 24 columnar and soft-crystalline orthorhombic, monoclinic, and triclinic phases can be stabilized when two or three waves have nonparallel wave vectors. Their symmetry groups, molecular arrangements, and phase diagrams are worked out and used to identify the structures of the main observed bent-core phases and their various subphases.

DOI: 10.1103/PhysRevE.75.011706 PACS number(s): 61.30.Cz, 64.70.Md

I. INTRODUCTION

Liquid crystalline phases exhibit intermediate properties between isotropic liquids and solid crystals. Continuous rotational or translational symmetries characterize the rather simple properties of liquid states, whereas 230 discrete space groups yield a wide variety of behaviors in solids. The discovery of mesophases with two-dimensional (2D) and three-dimensional (3D) orders, on the one hand, and of ferroelectricity [1], on the other hand, has progressively blurred the borders between symmetry groups observed in solids and liquids. This tendency was reinforced after antiferroelectricity has been evidenced in systems of polar bent-core molecules [2]. In these systems eight main phases, denoted by $B1$ to $B8$ [3–9], with smectic, columnar, or 3D translational orders were rapidly identified, soon followed by numerous subphases. The smectic $B2$ phase [3,4] exhibits an antiferroelectric, tilted, and spontaneously chiral molecular organization [5] (space group $P222_1$). Smectic-CP (SmCP) [6] is an orthorhombic achiral analog of $B2$, in which the molecular planes are not tilted (space group $Pmma$). Besides, several orthorhombic and monoclinic two- or three-dimensional ordered structures, denoted by $B1$ and $B3$ to $B8$, have been evidenced below the one-dimensional phases or below the isotropic liquid. These phases are experimentally identified by their textures, and each of them often exhibits distinct physical properties in different compounds, which possibly yield an extension of the bent-core polymorphism to Bn subphases. For instance, several "phases" present either antiferroelectric or ferroelectric switching behaviors or even chiral or achiral symmetries.

A complete phenomenological account of this polymorphism is not yet available. In conventional mesophases, the phenomenological theories involve three main ingredients: a second-rank tensor breaking the continuous rotational symmetry of the isotropic liquid, a density wave accounting for the smectic layers formation, and the polarization and tilt vectors. They represent order parameters associated with the classical sequence of transitions: Isotropic $\rightarrow$ Nematic $\rightarrow$ SmA $\rightarrow$ Sm$C^{(*)}$, etc., involving successive simple ordering processes. Using density waves for explaining the formation of smectic layers, and then vectors for the in-layer polar and tilt orders, is quite similar to the classical approach in solids [10]. An alternative to this two-step approach is possible in bent-core antiferroelectric mesophases, in which the stabilization of the smectic $B2$ and SmCp phases may come from a *direct condensation of a transverse vector wave in the isotropic liquid* [11]. When the condensed wave is linearly polarized, an achiral nontilted antiferroelectric smectic phase (denoted by R) is stabilized. Its structure and symmetry correspond to those observed in SmCP. When the wave is elliptically polarized, the antiferroelectric smectic phase (denoted by EL) becomes spontaneously chiral and tilted. It has the same structure as that observed in $B2$. Furthermore, we have tentatively proposed that the nonsmectic circular phase, denoted by C and stabilized when the vector wave is circularly polarized, describes the underlying one-dimensional structure of the intriguing modulated $B7$ phase.

These phases are associated with a single branch in the infinite star $\vec{k}^*$ of the wave vector $\vec{k}$. The corresponding molecular order varies consequently along a single space direction. To stabilize two- and three-dimensional phases, the condensation of an increasing number of wave vectors belonging to $\vec{k}^*$ becomes necessary. When two nonparallel waves are active, columnar phases are stabilized whereas three noncoplanar waves lead to 3D soft crystals. Thus, a single condensation mechanism could explain the polymorphism observed in a whole class of bent-core mesophases. However, starting from the isotropic liquid yields tedious calculations and provides a too rich and useless variety of low-symmetry phases. We present here a simplified approach in which, starting separately from R, C, or EL, further symmetry breakdowns are provoked by additional vector waves normal to $\vec{k}$. As we shall presently see, this is sufficient to account for the observed polymorphism in almost all bent-core materials. Moreover, this simplified approach is less restrictive, since it describes also phases resulting from longitudinal vector and density waves condensation. We use the Landau theory in order to predict molecular structures and phase diagrams. The methods worked out in this article are closer to those used in solid crystals than to the conventional approach in liquid crystals. In particular, we apply the full machinery of space groups and their irreducible representations. The wide polymorphism and the structural features of bent-core materials require this systematic use of classical crystallographys.

Group theory plays an important role for determining the structure and the symmetry of the parent-phase elementary instabilities. To each such instability is associated a given order parameter, a list of stable phases, and the corresponding phase diagrams. Starting from the isotropic phase, the elementary instabilities are represented by tensor-wave order parameters. Two tensors with distinct ranks or distinct polarizations (e.g., longitudinal or transverse) correspond then to different instabilities. On the contrary, when studying the instabilities of the ordered *R*, C, and EL phases, tensor waves with distinct ranks may correspond to a single instability. For instance, a scalar density wave and a longitudinal polarization wave have the same symmetry in *R*, so that both can be equivalently used as the order parameter of the transition associated with this corresponding instability. In fact, both simultaneously onset at the critical temperature and, at the phenomenological point of view, choosing one of them as the order parameter is arbitrary (though in a given material one of these waves may physically play the central role). This means that using either a density wave or a polarization wave yields the same phases with qualitatively the same physical properties and phase diagrams. We shall generically use the expression "wave type" to represent the set of equivalent tensor waves associated with a single instability. For instance, in *R* density and longitudinal polarization waves are of the same type. The group theoretical analysis yielding the list of wave types for each high-symmetry phase is presented in the Appendix. In the following sections, we keep only the symbols of the irreducible representations to label the wave types (e.g., density and longitudinal polarization waves along *Ox* in *R* belong to the "A_1" ($\vec{e}_x$) wave type).

The detailed properties of the relevant stable phases, primarily their behaviors under electric field, will be presented elsewhere. The present work is not, however, restricted to drawing up lists of phases, space groups, and group/subgroup relationships. It can be used for refining the molecular structure models. Indeed, although much effort has been initially paid to identifying the structures and space groups of the *Bn* phases, until recently several structures remained unknown, so that the macroscopic characterization based on electro-optic properties and textures is still preferentially used to classify the different bent-core mesophases. Let us finally stress that, despite the accumulation of experimental data in the past decade, numerous contradictory theoretical or heuristic models are still competing. Confronting them with columnar and soft-crystalline phases could permit one to evaluate these models.

The second section of the article presents the vector-wave model. The two following sections are devoted to the enumeration of the 2D and 3D phases stabilized by progressive ordering in the smectic phases *R* and EL, together with their space groups and the corresponding phase diagrams. The methods used to complete this analysis are briefly presented in the first example of the phase A_1^x worked out in Sec. III. They use standard techniques of the phenomenological theory of phase transitions. For the other phases, we only present the main qualitative results of this analysis, symmetry, structures, and topological characteristics of the phase diagrams (order of the transition lines, number and nature of critical points). In the last section, we discuss the identification of the theoretical stable phases with observed structures and compare our approach with models available in the literature.

II. THE VECTOR-WAVE MODEL

All the elementary structural instabilities of the isotropic liquid state are, according to the Landau theory of phase transitions [12], associated with the condensation of tensor waves. Such waves are described, on the one hand, by their wave vector $\vec{k}$ and, on the other hand, by the rank "*r*" and the polarization of their tensor [13]. In this respect, two cases must be distinguished: (i) For $\vec{k}=0$, the order parameters are homogeneous tensors [14]. The ordered nematic phases are then anisotropic but remain homogeneous, and (ii) for $\vec{k}\neq 0$, inhomogeneous periodic structures can be stabilized. For instance, the smectic-*A* phase is induced by the condensation of a scalar ($r=0$) density wave [15]. Within a given elementary mechanism, one has to consider similar waves propagating in all the directions. Indeed, the star $\vec{k}^*$ of the wave vector contains infinitely many branches $\vec{k}$ located on the sphere $k=|\vec{k}|=$constant in the reciprocal space. In the simplest case when only two opposite branches of the star condense at the transition, the ordered phase has the structure of a 1D wave with a period $\lambda=2\pi/k$.

Before presenting the way we deal with vector waves ($r=1$), let us first recall the similar case of the Sm*A* phase formation [16]. The layer structure of Sm*A* results from the condensation of a 1D scalar ($r=0$) density wave $\delta\rho_k$,

$$\delta\rho_{\vec{k}}(\vec{r}) = \eta_{\vec{k}} e^{i\vec{k}\cdot\vec{r}} + \eta_{-\vec{k}} e^{-i\vec{k}\cdot\vec{r}}. \tag{1}$$

Although the order parameter is formally infinitely dimensional, the transition is described by only two "effective" components, $\eta_{\vec{k}}$ and $\eta_{-\vec{k}}=\eta_{\vec{k}}^*$, associated with the pair of branches ($\pm\vec{k}$) active in $\vec{k}^*$. The same order parameter permits further stabilizations of two- and three-dimensional ordered structures when several density waves with nonparallel wave vectors condense simultaneously. The density field reads then

$$\rho(\vec{r}) = \rho_0 + \sum_{\vec{k}} \delta\rho_{\vec{k}}(\vec{r}),$$

where the sum runs over the active branches of the star. The stable phases have discrete periodic symmetries in two or three dimensions together with discrete point groups.

A similar approach may be used to account for antiferroelectricity in bent-core liquid crystals. A transverse vector wave belonging to an infinite-dimensional order parameter is then involved in the condensation process instead of the density wave. The simplest phases stabilized are then one-dimensionally periodic and antiferroelectric [11] because only two wave vectors ($\pm\vec{k}$) are active in $\vec{k}^*$. Their structures can be described by means of an effective order parameter that has only four components, η_1, η_2, η_1^*, and η_2^* defined by [see Eq. (1)].

$$\vec{P}(\vec{r}) = (\vec{e}_x + i\vec{e}_y)\{\eta_1 e^{i\vec{k}\cdot\vec{r}} + \eta_2 e^{-i\vec{k}\cdot\vec{r}}\} + (\vec{e}_x - i\vec{e}_y)\{\eta_1^* e^{-i\vec{k}\cdot\vec{r}} + \eta_2^* e^{i\vec{k}\cdot\vec{r}}\}, \quad (2)$$

where the polar vector wave $\vec{P}(\vec{r})$ represents the mean local polarization associated with the bent-core twofold molecular axis ordering. $\vec{e}_x$ and $\vec{e}_y$ are unit vectors parallel to Ox and Oy, respectively. The vector wave $\vec{k}$ is a phenomenological parameter that must be determined experimentally or calculated within microscopic models. $\vec{P}(\vec{r})$ is coupled with an axial wave $\vec{A}(\vec{r})$ representing the tilt of the molecular plane with respect to the direction of the wave vector which constitutes a "pseudoproper order parameter [17] ." The molecular orientations are determined by the equilibrium amplitudes and phases of these two waves. Three "unprimed" phases (displayed in Fig. 1) can first be stabilized when the phases of the two waves are locked:

(i) The "circular" C phase, in which $\vec{P}(\vec{r})$ and $\vec{A}(\vec{r})$ are circularly polarized. Its symmetry group $\infty_1 22$ (continuous group of a regular helix) yields a structure remaining homogeneous (no density wave) and macroscopically isotropic in the plane normal to $\vec{k}$. We have proposed [11] that this chiral helielectric nonsmectic phase corresponds to the 1D approximation of $B7$ when one neglects the long wavelength modulation normal to the main periodicity direction. Setting $\vec{k}$ along Oz, the polarization and tilt waves read then

$$\vec{P}_C(\vec{r}) = P_C \begin{pmatrix} \cos(kz) \\ \sin(kz) \end{pmatrix}, \quad \vec{A}_C(\vec{r}) = A_C \begin{pmatrix} \cos(kz) \\ \sin(kz) \end{pmatrix} \quad (3)$$

in the x-y plane. P_C and A_C denote their real wave amplitudes, vanishing as $(T-T_c)^{1/2}$ at the C→Isotropic transition temperature T_c.

(ii) In the "linear" R phase, the right- and left-handed circular waves in Eq. (2) have the same amplitude so that;

$$\vec{P}_R(\vec{r}) = P_R \begin{pmatrix} \cos(kz) \\ 0 \end{pmatrix}, \quad \vec{A}_R(\vec{r}) = A_R \begin{pmatrix} 0 \\ \sin(kz) \end{pmatrix}. \quad (4)$$

Its discrete orthorhombic group $Pmma$ describes an achiral smectic phase, which can be either antiferroelectric or anticlinic. In the former case, the bent-core molecules align with their polarizations normal to Oz, forming the antiferroelectric two-layer sequence displayed in Fig. 1.

(iii) In the "elliptic" EL phase, the two circular waves forming $\vec{P}(\vec{r})$ in Eq. (2) have independent amplitudes, yielding a chiral, antiferroelectric, and anticlinic structure with symmetry $P222_1$. In this phase, the polarization and tilt fields,

$$\vec{P}_{EL}(\vec{r}) = \begin{pmatrix} P_x \cos(kz) \\ P_y \sin(kz) \end{pmatrix}, \quad \vec{A}_{EL}(\vec{r}) = \begin{pmatrix} A_x \cos(kz) \\ A_y \sin(kz) \end{pmatrix}, \quad (5)$$

coincide with the structure of the phase $B2$ [5,11].

When the phases of $\vec{A}(\vec{r})$ and $\vec{P}(\vec{r})$ are no longer locked together, additional 1D "primed" phases, denoted by C′, R', R'', and EL′ with symmetries ∞_1, $P2_1/m$, $Pmc2_1$, and $P21$, respectively, condense spontaneously.

Likewise in the solidification process, the condensation of several nonparallel wave vectors in the star of $\vec{k}$ leads to a large variety of 2D and 3D low-symmetry phases. The polar and axial vector waves read then $\Sigma\vec{P}_{\vec{k}}(\vec{r})$ and $\Sigma\vec{A}_{\vec{k}}(\vec{r})$, respectively, where the sums run over the active branches of the star $\vec{k}^*$. For instance, after the simultaneous condensations of three perpendicular wave vectors, at least 11 cubic phases with space groups $Pn3n$, $P4_132$, $P4_332$, $Fd3c$, $Fm3c$, $Ia3d$, $I432$, $Im3$, $I\bar{4}3d$, $Ia3$, and $I\bar{4}3m$ can be stabilized [18]. Similarly, two perpendicular wave vectors can give rise to the appearance of many quadratic phases. In addition, such perpendicular wave vectors permit also the stabilization of a number of less symmetric states. Finally, various other wave-vector configurations complete the list of possible ordered structures within the vector-wave model. However, in bent-core molecular compounds, neither cubic nor quadratic phases have yet been evidenced. The tedious classification of all the vector-wave stabilized phases is thus not necessary to account for the observed polymorphism. The bent-core 2D and 3D phases can be more simply obtained as subphases of C, R, and EL, by considering the condensation of one or two additional waves in these three states without referring to their common origin in the isotropic liquid. The symmetry groups of the 2D and 3D phases are then subgroups of $\infty_1 22$, $Pmma$, or $P222_1$, respectively, so they cannot have subphases with tetragonal or cubic symmetries. The corresponding list of possible stable phases remains quite large (24 phases) because (i) one has to consider three high-symmetry phases; (ii) for each one, the wave vectors can appear with various nonequivalent relative orientations; (iii) each wave vector is associated with tensors of various ranks; (iv) each rank yields several ordered phases; and (v) several equivalent waves can be simultaneously active.

In order to predict the molecular arrangements, it is necessary to work out, in addition to $\vec{P}$ and $\vec{A}$, the lowest harmonics of the density, which determines the most probable positions of the molecules in the unit cell. In the smectic stable phases, the period of the density wave is half that of the vector waves. In 2D and 3D structures, density waves are induced in the same directions as the vector waves are.

The molecules are located at symmetric positions in the unit cell where the density function is maximum. For instance, in the R phase, the density maxima can coincide either with those of $\vec{P}$ or with those of $\vec{A}$. These possibilities define two configurations of the same phase, exhibiting different physical properties [11]. In the first case, the structure is antiferroelectric and not tilted (Fig. 1), whereas in the other case the structure is anticlinic with approximately zero local polarization. The same diversity arises in the higher dimensional mesophases. In a given stable phase, the symmetry analysis alone cannot foresee which configuration will be actually stable, since it depends on the sign of the coupling coefficients between polarization and density waves. Therefore, the thermodynamic analysis assigns different regions of the phase diagram to each variant of a single phase.

III. SUBPHASES OF SmCP

When additional vector waves (with wave vectors $\vec{K}$ normal to $\vec{k}$) condense, the linear R phase (i.e., SmCP) can

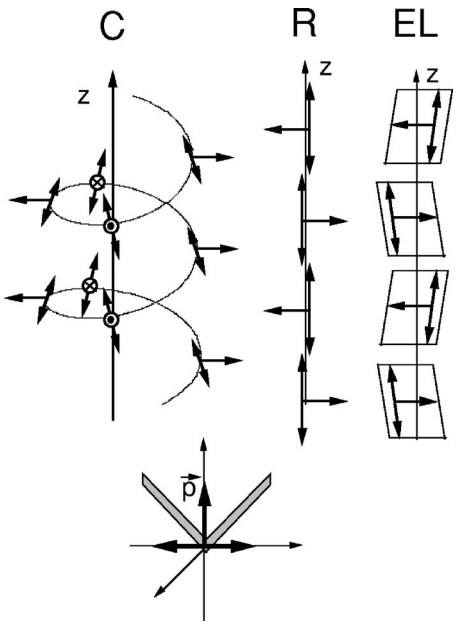

FIG. 1. Molecular structures of the one-dimensional circular (C), linear (R=SmCP) and elliptic (EL=$B2$) phases. All the molecules lying in one plane normal to O_z have the same orientation. One bent-core molecule is represented with one vector and one two-end arrow. The mean polarization $\vec{P}(\vec{r})$ is parallel to the molecular polarization shown in the figures by a one-end arrow. The tilt vector $\vec{A}(\vec{r})$ is parallel to the rotation axis turning the molecular plane from its reference orientation (parallel to the vector wave $\vec{k}$ and the polarization) to its actual configuration shown in the figure. One sees that in C and EL $\vec{A}(\vec{r})$ is parallel to $\vec{P}(\vec{r})$ and cancels in R (at least where the molecules are represented). In R and EL, only the molecules located at the maxima of the density wave (i.e., in the smectic planes) are represented. We have pictured the antiferroelectric configuration of R, in which the molecules lying in the smectic planes are not tilted (whereas molecules located between the planes are tilted). In the anticlinic configuration (not represented), the molecules in the smectic planes are not polarized on the average (due to statistical jumps between opposite values of the polarization), but they are tilted.

undergo various transitions toward columnar or 3D phases. All the corresponding elementary instabilities are driven by scalar or vector waves giving additional contributions to the structural fields $\vec{P}(\vec{r})$, $\vec{A}(\vec{r})$, and $\rho(\vec{r})$.

Let us illustrate these mechanisms with the simplest cases of waves condensing along the direction Ox parallel to the polarization in R, as follows:

(i) A density wave, $\delta\rho(x)$, breaks the homogeneity of the smectic planes along Ox, but it preserves the homogeneity along Oy, so that a columnar phase is stabilized with its columns parallel to Oy. In the smectic planes, the molecules are concentrated around the maxima of the wave. Due to the breakdown of the continuous translations along Ox, the molecules at the maxima and those between the maxima of the density wave are no longer equivalent. Accordingly, the mean polarization at the maxima and out of the maxima become different, but they both remain parallel to Ox because the twofold axis fixing the polarization direction in R is not broken by the density wave. This modulation $\delta P(x)\,\vec{e}_x$ along Ox of the polarization parallel to Ox corresponds to the condensation of a longitudinal polarization wave, which is induced by the "primary" condensation of the density wave. Reciprocally, one sees immediately that the spontaneous condensation of such a polarization wave induces the density wave. This means that the two waves are thermodynamically and symmetrically equivalent (technically, span the same irreducible representation of the R space group). In the language of the theory of phase transitions, one says that the density and polarization waves are pseudoproper order parameters. We shall say more simply that they are of the same wave type [namely, $A_1(\vec{e}_x)$]. The fact that they appear simultaneously is related to the presence of a bilinear coupling term in the free energy [I_3 in Eq. (7)] between the amplitudes of the two waves. This term is proportional to the phase shift between the maxima of the two waves along Ox, so that two distinct ordered phases can be stabilized. When the phase shift vanishes (coincidence between the maxima), an apolar "unprimed" phase appears. When the phase shift becomes finite, the symmetry of the unprimed phase is further broken, which stabilizes a polar "primed" phase. Infinitely many other pseudoproper tensor waves have in fact the same $A_1(\vec{e}_x)$ type and appear also at the transition. However, they cannot stabilize additional less symmetric phases and so can be firstly ignored in the thermodynamic description.

(ii) On the contrary, a longitudinal tilt wave $\delta A(x)\vec{e}_x$, which represents the tilt of the molecular plane around Ox with respect to its x-z locked value in R, breaks the x-z mirror plane of the polarization wave. Thus, this axial wave has a different type as $A_1(\vec{e}_x)$ and defines an independent elementary instability, which provokes an anticlinic tilting of the structure in the direction Ox.

(iii) Finally, transverse axial and polar waves define the two remaining independent elementary instabilities of the R phase associated with waves along Ox.

As stated in the previous section we shall usually assume that in the isotropic liquid $\vec{K}$ belongs to the star $\vec{k}^*$, so that one has $|\vec{K}| \approx |\vec{k}|$. This equality yields low-symmetry phases with formally tetragonal unit cells. In fact, these unit cells are actually rectangular, for the corresponding space groups are orthorhombic or monoclinic. The rectangular deformation of the tetragonal cell results from the onset of secondary homogeneous strain tensors induced by the primary tensor waves. The previous equality of the wave-vector lengths is convenient for presenting geometrical and analytical results in a compact form. We shall discuss its relation to the experimental situation in Sec. VI. The present section is devoted to the enumeration and description of the ordered phases arising below R. The procedure used to obtain space groups and molecular arrangements is worked out in detail in the case of the phase denoted by A_1^x, which coincides with the $B1$ bent-core columnar phase.

In R three nonequivalent directions in the x-y plane (normal to $\vec{k}$) must be considered.

(1) $\vec{K}=K_x\vec{e}_x$ is parallel to the plane of polarization in R (see Fig. 1). The star of $\vec{K}$ (set of wave vectors obtained from $\vec{K}$ after applying the point symmetries of R) has two branches

and the resulting low-symmetry phases are two-dimensional. $\vec{K}$ yields four nonequivalent wave types, denoted by $A_1(\vec{e}_x)$, $A_2(\vec{e}_x)$, $B_1(\vec{e}_x)$, and $B_2(\vec{e}_x)$.

(2) $\vec{K}=K_y\vec{e}_y$ is perpendicular to the polarization in R. The star has two branches and the low-symmetry phases are two-dimensional. The waves are again of the types $A_1(\vec{e}_y)$, $A_2(\vec{e}_y)$, $B_1(\vec{e}_y)$, and $B_2(\vec{e}_y)$.

(3) $\vec{K}=K_x\vec{e}_x+K_y\vec{e}_y$ lies in the general direction of the x-y plane. Its star contains four branches and the corresponding induced lattices are either 2D or 3D. Only two types of waves, denoted by R_+ and R_-, are permitted.

A. $\vec{K}=K_x\vec{e}_x$

For convenience $A_1(\vec{e}_x)$, $A_2(\vec{e}_x)$, $B_1(\vec{e}_x)$, and $B_2(\vec{e}_x)$ denote the four wave types. $A_1(\vec{e}_x)$ and $A_2(\vec{e}_x)$ are spanned by longitudinal polar (polarization) and axial (tilt) waves, respectively. $B_1(\vec{e}_x)$ [or $B_2(\vec{e}_x)$] is spanned by a transverse polar wave polarized along Oz [Oy] or equivalently by a transverse axial wave polarized along Oy [Oz]. Each wave leads to a single low-symmetry unprimed phase that we denote by A_1^x, A_2^x, B_1^x, and B_2^x. They have "nonminimal" orthorhombic symmetry groups belonging to the apolar D_{2h} class. Therefore, for each wave, the condensation of a second wave with the same type is necessary to complete the symmetry-breaking process (see, e.g., Ref. [19]), i.e., to stabilize minimal symmetry groups associated with this wave type. The corresponding "reducible" order parameters yield two distinct ordered phases for each wave type. The additional "primed" phases, denoted by $A_1^{x\prime}$, $A_2^{x\prime}$, $B_1^{x\prime}$, and $B_2^{x\prime}$, remain orthorhombic but in the polar C_{2v} class. Indeed, when the phases of the two complex wave amplitudes are shifted (we say that the two order parameters are not "parallel"), the mirror symmetry normal to $\vec{K}$ is broken. The primed phases are spontaneously ferrielectric along Ox though they remain achiral. Their space groups are listed in Table I.

The form of the free energy accounting for the thermodynamic features of the transition is the same for each of the four wave types. So, let us present it in the case of the $A_1(\vec{e}_x)$ wave type, and let $\psi=\rho e^{i\theta}$ and $\psi'=\rho' e^{i\theta'}$ denote the complex amplitudes of two such waves (e.g., a density wave and a longitudinal polarization wave with the same wave vector $\vec{K}=K_x\vec{e}_x$). ψ represents the complex amplitude of the density wave along Ox [$\delta\rho(x)$] whereas ψ' is the amplitude of the longitudinal polarization wave [$\delta\vec{P}(x)$],

$$\delta\rho(x) = \rho e^{i(K_x x+\theta)} + \rho e^{-i(K_x x+\theta)},$$

$$\delta\vec{P}(x) = i(\rho' e^{i(K_x x+\theta')} - \rho' e^{-i(K_x x+\theta')})\vec{e}_x. \tag{6}$$

In the unprimed phase, θ and θ' are locked, $\theta=\theta'+n\pi$ with n an integer, whereas the primed phase is associated with generic values of θ and θ'. The free energy F depends on the three invariant polynomials, $I_1=\psi\psi^*$, $I_2=\psi'\psi'^*$, and $I_3=\psi\psi'^*+\psi'\psi^*=2\rho\rho'\cos(\theta-\theta')$,

$$F = a_1 I_1 + a_2 I_2 + a_3 I_3 + a_{11} I_1^2 + a_{22} I_2^2 + a_{33} I_3^2 + a_{12} I_1 I_2 + \cdots . \tag{7}$$

I_1 and I_2 separately give the condensation energies associated with the density and polarization waves. The coupling term I_3 tends to lock the phase shift between the two waves (in A_1^x), and controls its temperature variation when the locking fails (in $A_1^{x\prime}$). Minimization of F with respect to ρ, ρ', and $\theta-\theta'$ yields the equilibrium equations of state of the ordered phases,

$$\begin{pmatrix} \rho & 0 & \rho'\cos(\theta-\theta') \\ 0 & \rho' & \rho\cos(\theta-\theta') \\ 0 & 0 & \rho\rho'\sin(\theta'-\theta) \end{pmatrix} \begin{bmatrix} a_1 + 2a_{11}I_1 + a_{12}I_2 + \cdots \\ a_2 + 2a_{22}I_2 + a_{12}I_1 + \cdots \\ a_3 + 2a_{33}I_3 + a_{13}I_1 + \cdots \end{bmatrix} = 0. \tag{8}$$

Their stability conditions $d^2F \geqslant 0$ yield the phase diagrams depicted in Fig. 2. The simplest complete phase diagram in which the three phases have extended domains of stability is obtained with the "canonical" free energy (Morse function of the invariants I_1, I_2, and I_3),

$$F_{\text{can}} = \sum_i a_i I_i + \frac{b_i}{2} I_i^2.$$

The $R \to A_1^x$ and $A_1^x \to A_1^{x\prime}$ transition lines are then always second order. Their equations are given by

$$4a_1a_2 = a_3^2 \quad (a_1, a_2 \geqslant 0),$$

$$\frac{a_1a_2}{\sqrt{b_1b_2}} = \frac{a_3^2}{b_3} \quad (a_1, a_2 \leqslant 0). \tag{9}$$

a_1, a_2, and a_3 are linear functions of the external fields, say temperature T and concentration c: $a_i=a_{io}+a_{iT}T+a_{ic}c$, whereas a_{io}, a_{iT}, a_{ic}, and b_i are constant parameters to be determined experimentally. Varying T in the neighborhood of the $R \to A_1^x$ transition line allows us to write $a_i=\alpha_i+\lambda_i(T_c-T)$, where $\alpha_i=a_i(T_c)=a_{io}+a_{iT}T_c+a_{ic}c$. Solving Eqs. (8) gives then the thermodynamic behavior of the polarization and density waves amplitudes,

$$\rho^2 = 2\frac{\alpha_1\lambda_2 + \alpha_2\lambda_1}{(s-2)\alpha_1 - (s+2)\alpha_2}\frac{T_c - T}{\alpha_1},$$

$$\rho'^2 = 2\frac{\alpha_1\lambda_2 + \alpha_2\lambda_1}{(s-2)\alpha_1 - (s+2)\alpha_2}\frac{T_c - T}{\alpha_2}, \tag{10}$$

where $s=b_3/\sqrt{b_1b_2}$. The ratio relating the two amplitudes depends only on the quadratic coefficients α_i: $\rho/\rho'=\sqrt{\alpha_2/\alpha_1}$. Thus, when $\alpha_2 \gg \alpha_1$, the transition is mainly driven by the density wave ρ, while in the opposite case $\alpha_2 \ll \alpha_1$, the dominant mechanism is the condensation of the longitudinal polarization wave ρ'.

When higher-degree polynomials are taken into account in the free energy (7), a direct first-order transition becomes possible between R and $A_1^{x\prime}$. The corresponding transition line is limited by two tricritical points and crosses the $A_1^x \to A_1^{x\prime}$ transition line at two three-phase points. The axes of the phase diagrams depend linearly on two external ther-

TABLE I. List of phases stabilized below the linear R phase (SmCP) when $\vec{K}$ is parallel to $\vec{e}_x$. The first column indicates the wave type. The second column indicates the nature of the waves. The third and fourth columns indicate the names and space groups of the unprimed and primed phases, respectively. The letter between parentheses indicates the direction parallel to the rotation axis or normal to the mirror plane: e.g., in $Pm(y)c(z)2_1(x)$ the gliding plane "c" is normal to Oz, the mirror plane m is normal to Oy, and the twofold screw axis 2_1 is parallel to Ox.

	Vector waves	Phases A_i/B_i	Phases A_i'/B_i'
$A_1(\vec{e}_x)$	Longitudinal polar	A_1^x: $Pmma(x)$ D_{2h}^5	$A_1^{x\prime}$: $Pmm2(x)$ C_{2v}^1
$A_2(\vec{e}_x)$	Longitudinal axial	A_2^x: $Pcca(x)$ D_{2h}^8	$A_2^{x\prime}$: $Pcc2(x)$ C_{2v}^3
$B_1(\vec{e}_x)$	Transverse	B_1^x: $Pb(z)a(x)m(y)$ D_{2h}^9	$B_1^{x\prime}$: $Pm(y)c(z)2_1(x)$ C_{2v}^2
$B_2(\vec{e}_x)$	Transverse	B_2^x: $Pb(y)c(x)m(z)$ D_{2h}^{11}	$B_2^{x\prime}$: $Pm(z)c(y)2_1(x)$ C_{2v}^2

modynamic parameters such as temperature and concentration. When only the temperature varies, the equilibrium state moves along a straight line in the phase diagram, giving rise to the "normal" sequence $A_1^{x\prime} \rightarrow A_1^x \rightarrow R$ or the reentrant sequence $A_1^x \rightarrow A_1^{x\prime} \rightarrow A_1^x \rightarrow R$. The same free energy (7) and the corresponding phase diagrams hold also for the waves $A_2(\vec{e}_x)$, $B_1(\vec{e}_x)$, and $B_2(\vec{e}_x)$.

Let us describe the vector fields and molecular structures of the unprimed phases. The polarization and tilt $\vec{P}(x,z)$ and $\vec{A}(x,z)$ together with the density $\rho(x,z)$ depend on x and z. Using the fact that $A_1(\vec{e}_x)$ is spanned by a longitudinal polar wave, $A_2(\vec{e}_x)$ by a longitudinal axial wave, B_1 and B_2 by polar (or equivalently axial) transverse waves, and keeping only the lowest harmonics, $\vec{P}(x,z)$ and $\vec{A}(x,z)$ read (in the domains defined by $\theta=\theta'=0$, and setting for simplicity $|\vec{K}|=|\vec{k}|=1$),

$$A_1^x: \quad \vec{P} = P_0 \sin(z)\vec{e}_x + \rho' \sin(x)\vec{e}_x,$$

$$\vec{A} = A_0 \cos(z)\vec{e}_y,$$

$$A_2^x: \quad \vec{P} = P_0 \sin(z)\vec{e}_x + \rho_1 \cos(x)\cos(z)\vec{e}_y,$$

$$\vec{A} = A_0 \cos(z)\vec{e}_y + \rho'' \sin(x)\vec{e}_x,$$

$$B_1^x: \quad \vec{P} = P_0 \sin(z)\vec{e}_x + \rho \sin(x)\vec{e}_z,$$

$$\vec{A} = A_0 \cos(z)\vec{e}_y + \rho'' \cos(x)\vec{e}_y,$$

$$B_2^x: \quad \vec{P} = P_0 \sin(z)\vec{e}_x + \rho' \sin(x)\vec{e}_y,$$

$$\vec{A} = A_0 \cos(z)\vec{e}_y + \rho'' \sin(x)\vec{e}_z,$$

where ρ'' represents the amplitude of the tilt wave having the same type as ρ (density) and ρ' (polarization). Close to T_c these three amplitudes are proportional. ρ_1 is a secondary order parameter vanishing in R. $\vec{P}$ and $\vec{A}$ do not completely characterize the structures of the ordered phases since they do not provide the positions of the molecules in the unit cell. Indeed, the molecules are mainly concentrated around the maxima of the density wave that we shall work out below. The extrema of $\vec{P}$ and $\vec{A}$ in the density lattice are not completely determined by the space groups, so that several nonequivalent structures with the same symmetry may be associated with each phase. Some examples of the corresponding waves and molecular structures are depicted in Fig. 3.

Let us take as an example the determination of the molecular positions in A_1^x. In this phase the first harmonics of the density read

$$\rho(x,z) = \rho_0 + \rho_z \cos(2z) + \rho \cos(x) + \rho_2 \sin(z)\sin(x), \tag{11}$$

where ρ_0 is the density in the isotropic liquid, ρ_z and ρ describe its smectic modulations in R and A_1^x, whereas ρ_2 is a nonsymmetry-breaking density wave that is induced in A_1^x by its coupling with ρ. One can easily show that ρ and ρ_2 vary in A_1^x as $(T_c-T)^{1/2}$ and (T_c-T), respectively (T_c denotes the $R \rightarrow A_1^x$ transition temperature). Three possible sets of density maxima are indicated in Fig. 3(a). The molecular orientations are determined by the corresponding local values of polarization and tilt at these points. In case (1) of Fig. 3(a) the positions of the molecules are fixed at symmetry points of the unit cell. In cases (2) and (3), the molecular positions vary with temperature along Oxz and Ox, respectively. The

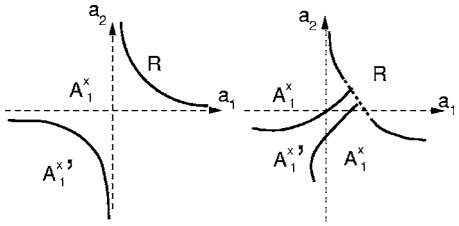

FIG. 2. Phase diagrams of the $R[\text{Sm}CP] \rightarrow A_1^x[B1]$ transition. This diagram holds also for the phases A_y^1 $A_2^{x,y}$, $B_1^{x,y}$, and $B_2^{x,y}$ (see Tables I and II). Continuous and broken lines indicate second- and first-order transitions, respectively. (a) When the free energy [Eq. (7)] is truncated up to the fourth degree. (b) When the free energy is truncated up to the sixth degree. The axes represent phenomenological coefficients defined in Eq. (7), which are combinations of two external parameters such as temperature and concentration. Varying only the temperature amounts to a move along straight lines in the diagrams.

structure (1) is purely anticlinic and cannot be obtained from the antiferroelectric variant of R presented in Fig. 1 and observed in the SmCP phase. In contrast, (1) can appear from the anticlinic variant of R after the condensation of the density wave $\rho\cos(x)$, which thus represents the primary order parameter of the transition. The vector wave $\rho'\sin(x)\vec{e}_x$ is then an induced secondary pseudoproper order parameter. On the contrary, in case (2), the antiferroelectric structure results from the condensation of the vector wave in the antiferroelectric variant of R displayed in Fig. 1. The molecular positions remain thus close to the maxima $x=z=\pm 1/4$ of the polarization, even though they can vary slightly around these maxima in the direction Ox. Therefore, the density waves are weak secondary pseudoproper or improper order parameters. In case (3), the structure is simultaneously anticlinic and antiferroelectric, and both waves participate to the ordering mechanism on the same footing.

A_1^x belongs to the same symmetry class $Pmma$ as the parent R phase does, but it has a 2D lattice instead of a 1D smectic structure. Thus, the polarization and tilt waves remain everywhere linearly polarized and perpendicular, though they become modulated along Ox. The maxima of $\vec{A}$ and $\vec{P}$ are shown in the two first columns of Fig. 3(b), whereas the molecular structures corresponding to the case (3) discussed above are shown in the third column. In case (3), the positions of the molecules coincide approximately with the maxima of $\vec{P}$ and the zeroes of $\vec{A}$, so that the tilt vanishes and the structure is almost purely antiferroelectric with two molecules in one unit cell. The corresponding primed $A_1^{x\prime}$ phase is ferrielectric because, although the polarizations direction remains frozen along Ox, the mean polarization magnitudes of two molecules in one unit cell become different. Indeed, due to the lost of the gliding plane of A_1^x normal to Ox, these two molecules are no longer equivalent in $A_1^{x\prime}$ with respect to fluctuations reversing the sense of the molecular polarization. In A_2^x when the molecules are located at the $\vec{P}$ maxima [Fig. 3(b)] the structure is antiferroelectric along Oz and anticlinic along Ox and Oz. In B_1^x the four molecular planes lie in the x-z plane, but their polarizations are turned around Oy. In B_2^x the planes of the two molecules are tilted around Oz.

B. $\vec{K}=K_y\vec{e}_y$

As above, each of the four types of waves, denoted by $A_1(\vec{e}_y)$, $A_2(\vec{e}_y)$, $B_1(\vec{e}_y)$, and $B_2(\vec{e}_y)$, leads to one orthorhombic nonpolar unprimed and one orthorhombic polar primed columnar phases, presented in Table II. The thermodynamic analysis and phase diagrams (Fig. 2) are the same as for $\vec{K}=K_x\vec{e}_x$. Two structures for each unprimed phase are drawn in Fig. 4. Although the space groups of A_1^x and A_1^y are nominally identical ($Pmma$), they are not actually isomorphic, so that A_1^x and A_1^y are distinct phases. Indeed, in A_1^x the gliding plane "a" (in $Pmma$) is normal to a direction of discrete translations (Ox since $\vec{K}$ is along Ox) while in A_1^y it is normal to the direction of continuous translations (Ox since in this case $\vec{K}$ is along Oy).

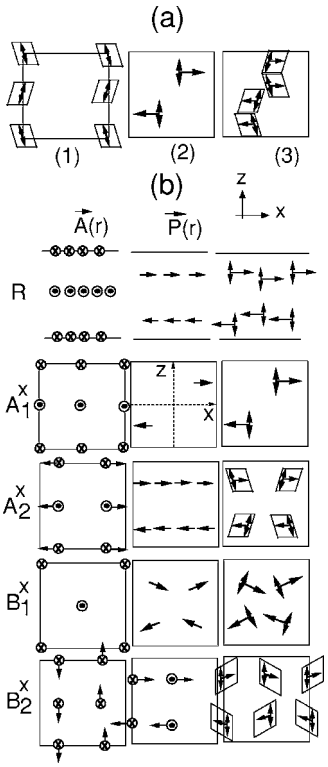

FIG. 3. (a) Molecular structures in three variants of the phase A_1^x. (b) Waves and molecular structures in one unit cell of the phases A_1^x, A_2^x, B_1^x, and B_2^x, (see Table I). The wave components normal to O_y are represented by in-plane arrows, whereas the parallel component is represented by circles. First column: Tilt fields $\vec{A}(x,z)$. Second column: Polarization fields $\vec{P}(x,z)$. Third column: Molecular configurations. The representation of single molecules is explained in Fig. 1.

C. $\vec{K}=K_x\vec{e}_x+K_y\vec{e}_y$

$\vec{K}=K_x\vec{e}_x+K_y\vec{e}_y$ permits two types of waves, denoted by R_+ (symmetric with respect to the mirror plane normal to $\vec{k}$) and by R_- (antisymmetric), respectively. R_+ may be spanned either by a density wave, a longitudinal polarization wave, a transverse polarization wave with $\vec{P}$ parallel to the smectic layers, or a transverse axial (tilt) wave with $\vec{A}$ normal to the smectic layers. R_- may be spanned either by a longitudinal tilt wave, a transverse polarization wave with $\vec{P}$ normal to the smectic layers, or a transverse axial (tilt) wave with $\vec{A}$ parallel to the smectic layers. In each case, the order parameter has four components ψ_1, ψ_2, ψ_1^*, and ψ_2^* associated with the four branches $\vec{K}_1=(K_x,K_y,0)$, $\vec{K}_2=(-K_x,K_y,0)$, $\vec{K}_3=(-K_x,-K_y,0)$, and $\vec{K}_4=(K_x,-K_y,0)$ of $\vec{K}^*$. ψ_1 and ψ_2 are thus the complex amplitudes of waves propagating along (K_x,K_y), and $(-K_x,K_y)$, respectively. The phases of ψ_1 and ψ_2 are Goldstone variables, which can be made to zero by suitably choosing the origin of the coordinates in the x-y plane. ψ_1 and ψ_2 represent then the real amplitudes of the waves along $\vec{K}_1$ and $\vec{K}_2$.

The free energy depends on two invariant polynomials, $I_1=\psi_1\psi_1^*+\psi_2\psi_2^*$ and $I_2=\psi_1\psi_1^*\psi_2\psi_2^*$. In contrast with the

TABLE II. List of phases stabilized below the linear R phase (SmCP) when $\vec{K}$ is parallel to $\vec{e}_y$. The first column indicates the wave type. The second column indicates the nature of the waves. The third and fourth columns indicate the names and space groups of the unprimed and primed phases, respectively.

	Vector waves	Phases A_i/B_i	Phases A_i'/B_i'
$A_1(\vec{e}_y)$	Longitudinal polar	A_1^y: $Pmma(y)$ D_{2h}^5	$A_1^{y\prime}$: $Pm(z)a(x)2(y)$ C_{2v}^4
$A_2(\vec{e}_y)$	Longitudinal axial	A_2^y: $Pm(y)n(x)a(z)$ D_{2h}^7	$A_2^{y\prime}$: $Pn(x)c(z)2(y)$ C_{2v}^6
$B_1(\vec{e}_y)$	Transverse	B_1^y: $Pmmn(x)$ D_{2h}^{13}	$B_1^{y\prime}$: $Pm(z)n(x)2_1(y)$ C_{2v}^7
$B_2(\vec{e}_y)$	Transverse	B_2^y: $Pb(z)c(x)m(y)$ D_{2h}^{11}	$B_2^{y\prime}$: $Pc(x)a(z)2_1(y)$ C_{2v}^5

waves ψ and ψ' traveling along Ox or Oy, studied in sections A and B there is no bilinear coupling between ψ_1 and ψ_2 so that a stable low-symmetry phase where ψ_1 (or equivalently in an equivalent domain ψ_2) cancels can be stabilized. The biquadratic coupling term I_2 permits the stabilization of this phase and leads, in the general case, to distinct values for the equilibrium amplitudes of the two waves. Minimizing the corresponding free energy $F(I_1,I_2)$ yields three ordered states for each wave type $R_\pm$,

(i) One columnar phase for $\psi_2=0$ (or $\psi_1=0$ in another domain) (denoted by $\mathrm{I}_\pm$).

(ii) One three-dimensional high-symmetry phase for $|\psi_1|=|\psi_2|\neq 0$ (denoted by $\mathrm{II}_\pm$).

(iii) One three-dimensional low-symmetry phase for $|\psi_1|\neq|\psi_2|\neq 0$ (denoted by $\mathrm{III}_\pm$).

Their orthorhombic and monoclinic space groups are presented in Table III. All the ordered phases are achiral and nonpolar. The phase diagrams are shown in Fig. 5. At the eighth-degree term approximation of the free energy, all the permitted transitions may be second order and the phases merge at a four-phase point. Higher-degree expansions permit direct first-order transitions from R to $\mathrm{III}_\pm$, the corresponding transition lines being surrounded by three-phase points. Some possible molecular structures and group-subgroup relationships are depicted in Fig. 6.

In the two next sections, we present similar mechanisms corresponding to instabilities of the chiral elliptic phase ($B2$). Since there is no fundamental difference with the mechanisms discussed above, we shall describe succinctly the classifications and shall enumerate the corresponding phases and space groups in several tables and figures.

IV. SUBPHASES OF $B2$

Any anisotropic perturbation of C transforms it into the elliptic phase, so that the condensation of waves in C yields the same subphases as their condensation in EL (i.e., $B2$). On the other hand, in many respects the situation in EL is similar to that in R, and one has again to consider wave vectors along Ox, Oy, and in the general direction of the x-y plane. However, since the chiral elliptic point group (D_2) is contained in the achiral linear point group (D_{2h}), the number of wave types in EL is divided by two with respect to that in R. The types denoted by A_1 and A_2 in R become equivalent in EL and give rise to a single type denoted by A, whereas B_1 and B_2 give rise to the type B. Analogously, the type R_+ becomes equivalent to R_-. Hence, each couple of R subphases (e.g., A_1^x and A_2^x) gives rise to a single subphase of EL. The chiral symmetry group of this single phase is the common subgroup of its two R analogs. For instance, the symmetry of the phase denoted by A^x, stabilized as a subphase of EL when $\vec{K}$ is parallel to Ox, is the intersection of the A_1^x and A_2^x space groups (see Table I). The molecular arrangement in A^x (Fig. 7) can be obtained from A_1^x by tilting the molecular

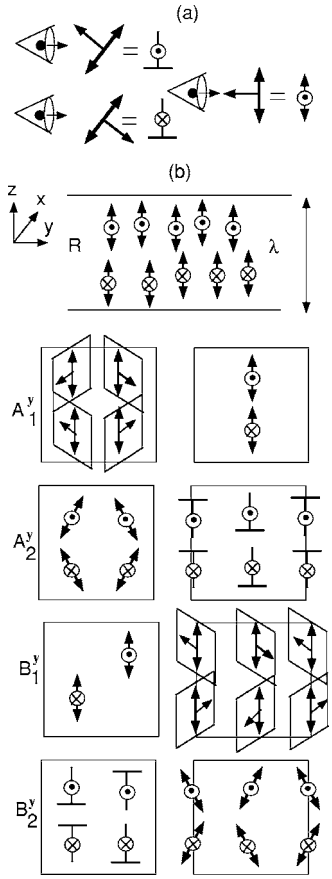

FIG. 4. Columnar subphases of R when $\vec{K}=K\vec{e}_y$. (a) Scheme of bent-core molecules seen from within their own plane. (b) Molecular arrangements in one unit cell of the phases R, A_1^y, A_2^y, B_2^y, and B_2^y (see Table II). The two columns display two variants of the same phase corresponding to two possible locations of the density maxima. The positions of the symmetry elements in the unit cell are the same in the two columns. In A_1^y (first column) and B_1^y (second column) the molecular polarizations are normal to O_z.

TABLE III. List of the phases stabilized below the linear R phase (SmCP) when $\vec{K}$ lies in the general direction of the x-y plane. The first column indicates the wave type. The second column indicates the nature of the waves. The following columns indicate the name and space group of the stable phases.

	Vector waves	$\psi_2=0$ ($I_\pm$)	$\lvert\psi_1\rvert=\lvert\psi_2\rvert\neq 0$ ($II_\pm$)	$\lvert\psi_1\rvert\neq\lvert\psi_2\rvert\neq 0$ ($III_\pm$)
R_+	Transverse longitudinal polar	$P2_1/m(z)$ C_{2h}^2 (2D)	$Cm(y)c(x)m(z)$ D_{2h}^{17} (3D)	$P2_1/m(z)$ C_{2h}^2 (3D)
R_-	Transverse longitudinal axial	$P2_1/b(z)$ C_{2h}^5 (2D)	$Cm(y)c(x)a(z)$ D_{2h}^{18} (3D)	$P2_1/b(z)$ C_{2h}^5 (3D)

planes around Ox, or equivalently from A_2^x by a disordering transition, which makes more likely one of the two equivalent molecular positions in each smectic layer (see Fig. 3). The three sets of ordered phases corresponding to $\vec{K}$ along Ox, Oy, and Oxy are listed in Tables IV and V, and their structures are depicted in Figs. 7 and 8.

A. $\vec{K}$ is parallel to Ox or to Oy

When $\vec{K}$ is parallel to Ox or to Oy, the unprimed structures are columnar, chiral, orthorhombic, and nonpolar, whereas the primed phases are columnar, chiral, monoclinic, and ferroelectric. The twofold rotation axes of the monoclinic phases are parallel to $\vec{K}$. A^x and A^y ($A'^{x,y}$, $B^{x,y}$, and $B'^{x,y}$) are distinct subphases of EL, though they have the same formal space group $P222_1$ ($P2_12_12$, $P2$, and $P2_1$). However, these phases can also be stabilized directly from C (or, similarly, from the nematic or the isotropic phases). In this case, A^x and A^y (or B^x and B^y, etc.) form two variants of a single phase. Consequently, close to the stability domain of EL in the phase diagram, A^x and A^y are necessarily separated by a first-order transition line. Far from EL, this line can possess a critical end point.

When the waves A and B appear together, two additional monoclinic phases (AB and AB_Z) and one triclinic phase (AB_0) can also be stabilized. Each of these phases has one x and one y variant. Their space groups are presented in Table V and some molecular structures are shown in Fig. 8.

$A(\vec{e}_x)$ is spanned either by a longitudinal vector wave $\delta\vec{P}(x)=\delta P_x\,\vec{e}_x$ or by a scalar wave $\delta\rho(x)$. Let us denote their complex amplitudes by $\eta^+=\rho_+e^{i\theta_+}$ and $\eta'_+=\rho'_+e^{i\theta'_+}$, respectively,

$$\delta P_x=(\eta_+e^{ix}-\eta_+^*e^{-ix}),\quad \delta\rho=(\eta'_+e^{ix}+\eta'^*_+e^{-ix}).$$

Likewise, $B(\vec{e}_x)$ is spanned by any of the two transverse vector waves ($\eta_-=\rho_-e^{i\theta_-}$, $\eta'_-=\rho_-e^{i\theta'_-}$),

$$\delta P_z=(\eta_-e^{ix}+\eta_-^*e^{-ix}),\quad \delta P_y=(\eta'_-e^{ix}+\eta'^*_-e^{-ix}),$$

where $\theta_\pm=\theta'_\pm+n\pi$ in the unprimed phases.

When one does not attempt to account for the primed phases, the free energy F may be written as a function of η_+ and η_- alone, and it reads in the fourth-order term approximation

$$F(\eta_+,\eta_-)=a_1I_1+a_2I_2+cI_3+\frac{a_{11}}{2}I_1^2+\frac{a_{22}}{2}I_2^2+a_{12}I_1I_2, \tag{12}$$

where $I_1=\eta_+\eta_+^*$, $I_2=\eta_-\eta_-^*$, $I_3=(\eta_+\eta_-^*)^2+(\eta_-\eta_+^*)^2$, with $a_{11}a_{22}>(a_{12}\pm c)^2$. The coupling term I_3 has no effect in the most symmetric phases A and B. On the other hand, it fixes $\theta_+=\theta_-$ or $\theta_+=\frac{\pi}{2}+\theta_-$ in the intermediate phases AB and it controls the temperature variation of $\theta_+-\theta_-$ in the least symmetric phase AB_0 [provided a term proportional to I_3^2 is added to the free energy (12) for stabilizing AB_0]. Figure 9 displays phase diagrams associated with Eq. (12). The triclinic phase AB_0 is not stable within this approximation. All the transition lines are second order and merge at four-phase points. The stable phase is AB when $a_3<0$ and AB_Z when $a_3>0$. The same free energy and phase diagrams are associated with $A(\vec{e}_y)$ and $B(\vec{e}_y)$.

B. $\vec{K}(K_x,K_y)$ is oriented along a generic direction in the x-y plane

When $\vec{K}(K_x,K_y)$ is oriented along a generic direction in the x-y plane, the order parameter has four components $(\psi_1,\psi_2,\psi_1^*,\psi_2^*)$, each one being spanned by a (density, transverse or longitudinal axial, or polar vector) wave along one of the four directions (K_x,K_y), $(-K_x,K_y)$, $(K_x,-K_y)$, $(-K_x,-K_y)$. It yields three ordered phases (Table VI) denoted by I_E ($\psi_2=0$ or $\psi_1=0$), II_E ($\lvert\psi_1\rvert=\lvert\psi_2\rvert$) and III_E ($\lvert\psi_1\rvert\neq\lvert\psi_2\rvert\neq 0$) analogous to the subphases $I_\pm$, $II_\pm$, and $III_\pm$ of R (see Table III). They are chiral and either orthorhombic (II_E) or

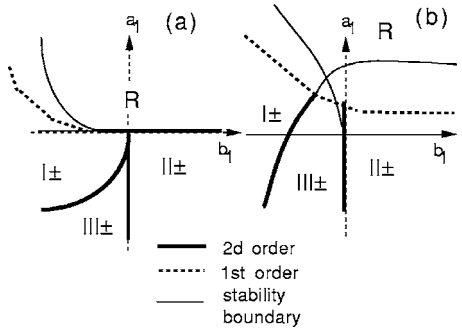

FIG. 5. Phase diagrams of the transitions R[SmCP] $\rightarrow I_\pm, II_\pm, III_\pm$ (see Table III). The axes represent phenomenological coefficients, which are linear combinations of two external parameters such as temperature and concentration.

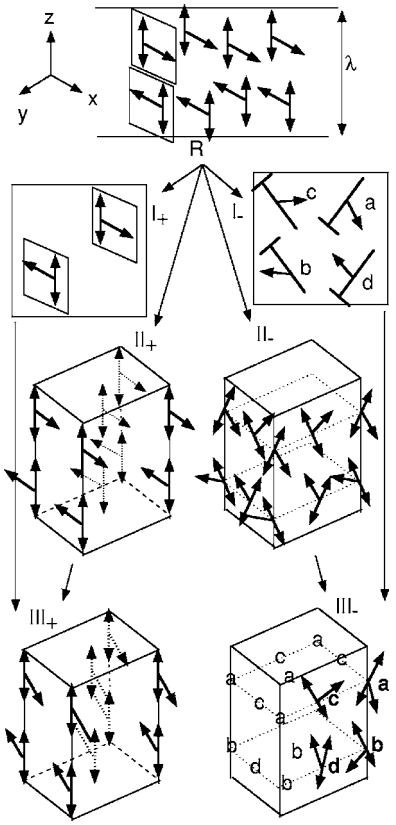

FIG. 6. Molecular structures and group-subgroup relationships between the phases $I_{\pm}$, $II_{\pm}$, $III_{\pm}$ (Table III). The conventional orthorhombic unit cells depicted for the 3D phases $II_{\pm}$ and $III_{\pm}$ contain two primitive cells. In II_{+} the molecular polarizations are parallel to O_x and the molecular planes are in the x-z plane. In III_{+} the polarizations are rotated around O_x in the x-y plane. In II_ and II_ only the molecules lying within the visible sides of the cell are represented. The molecular planes are parallel to x-z. In I_ and III_ the orientation of the molecule (a) is not locked along symmetric directions and it can change with temperature. The orientation of (b) is obtained from that of (a) after a twofold rotation around O_z. The orientation of (c) is obtained after a mirror symmetry transformation with respect to the x-y plane. The orientation of (d) is obtained from (a) by space inversion.

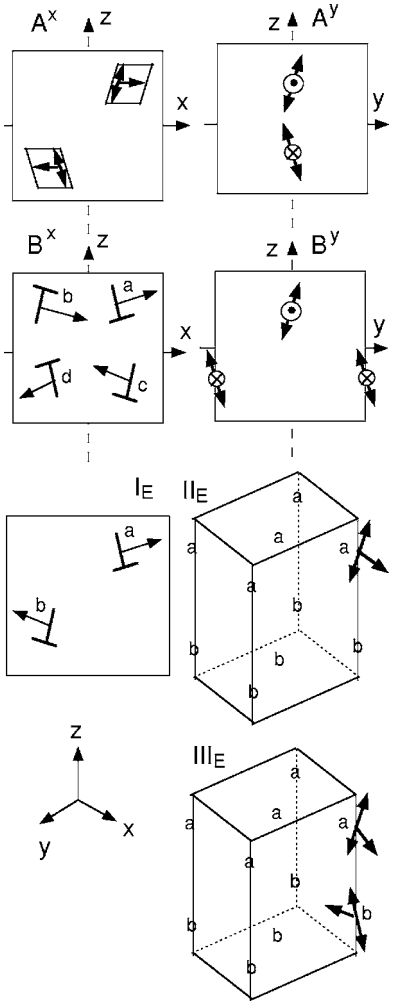

FIG. 7. Unit cell in subphases (Tables IV and V) of EL[$B2$]. In B^x the molecular polarizations $\vec{p}_{q=a,b,c,d}$ are in fact out of the x-z plane. The orientations of the molecules (b), (c), and (d) are obtained from that of (a) by applying the twofold rotations C_{2x}, C_{2y}, and C_{2z}, respectively: $\vec{p}_a=(p_x,p_y,p_z)$, $\vec{p}_b=(p_x,-p_y,-p_z)$, $\vec{p}_c=(-p_x,p_y,-p_z)$, $\vec{p}_d=(-p_x,-p_y,p_z)$. In I_E, II_E, and III_E, the molecules (b) are turned by C_{2z} with respect to the molecules (a). In II_E the molecular polarizations are along Ox whereas in I_E and III_E they have three independent components: $\vec{p}_a=(p_x,p_y,p_z)$, $\vec{p}_b=(-p_x,-p_y,p_z)$.

monoclinic (I_E and III_E). I_E is columnar whereas II_E and III_E form three-dimensional lattices.

The structure of EL is actually incommensurate [11]. Indeed, a spatial direction in the x-y plane (which would be fixed if EL were commensurate, e.g., Ox) precesses in fact slowly around $\vec{k}$ in the incommensurate structure. The additional wave vector $\vec{K}$ being normal to $\vec{k}$, the same precession must affect the large-scale structures of the 2D and 3D subphases of EL. A similar situation arises when a smectic density wave condenses in the modulated cholesteric state, yielding twist-grain-boundaries (TGB) superstructures. Similarly, we expect either TGB-type behavior or unwinding of the incommensurate EL modulation at the EL→higher-dimensional phases.

In the previous sections, we described 24 2D and 3D phases generated by the condensation, in the three one-dimensional vector-wave phases, of one or two waves normal to the helical axis. These structures are related by group-subgroup relationships summarized in Fig. 10. Most phases have an orthorhombic symmetry compatible with the rectangular unit cell observed in several bent-core structures. Considering wave vectors not perpendicular to the helical axis would lead to low-symmetry phases with nonrectangular cells.

V. DISCUSSION

A. Experiments

Any ordered phase may be, in principle, identified by its space group. The refinement of the motif (position and organization of the molecules in the unit cell) is then independent

TABLE IV. List of the phases stabilized below the elliptic EL phase ($B2$) when $\vec{K}$ is parallel to $\vec{e}_y$ or $\vec{e}_x$. The first column indicates the wave type. The second column indicates the nature of the waves. The third and fourth columns indicate the names and space groups of the unprimed and primed phases, respectively.

	Vector waves	Phases A/B	Phases A'/B'
A $(\vec{K}=\vec{e}_x)$	Longitudinal	A^x: $P222_1(z)$ D_2^2	A'^x: $P2(x)$ C_2^1
B $(\vec{K}=\vec{e}_x)$	Transverse	B^x: $P2_12_12(y)$ D_2^3	B'^x: $P2_1(x)$ C_2^2
A $(\vec{K}=\vec{e}_y)$	Longitudinal	A^y: $P222_1(z)$ D_2^2	A'^y: $P2(y)$ C_2^1
B $(\vec{K}=\vec{e}_y)$	Transverse	B^y: $P2_12_12(x)$ D_2^3	B'^y: $P2_1(y)$ C_2^2

of the phase identification since, as we have seen in the previous sections, several motifs can be attributed to a single space group. However, the symmetries are difficult to evidence experimentally, mainly because it is difficult to stabilize large single domains in most bent-core phases. Thus, one has to use indirect and incomplete information revealing the symmetry groups. In this section, we use available experimental data reporting (i) the group-subgroup relationships deduced from the observed sequences of phases (in most of the cases, on decreasing temperature the least symmetric phase appears at the end of the sequence), (ii) x-ray diffraction data, and (iii) electro-optic properties that provide some insight into the point groups and the motifs of the ordered phases.

The identification of the smectic $B2$ and SmCP phases with EL and R, respectively, is supported by the experimental refinement of their molecular organizations [5,6,11]. $B8$ is a tilted 1D phase presenting antiferroelectric switching that appears in the sequence Crystal → Sm0 → $B8$ → Isotropic liquid [20]. Although the structures of Sm0 and $B8$ seem similar to that of $B2$, their optical textures show helical superstructures distinguishing clearly the three phases. Moreover, Bragg reflections at $q/2$ indicate a bilayer structure in $B8$ that is not seen in $B2$ or Sm0. Since it differs from $B2$, the only chiral candidate for Sm0 is the primed elliptic EL′ phase (space group $P2_1$), which is stabilized when the complex amplitudes of two copies of the vector wave [see Eq. (5)] are not "parallel" (i.e., have different phases) [21]. The molecular polarizations remain antiferroelectric in the plane of the smectic layers, but they become ferroelectric in the direction of the helical axis. In EL′ the monoclinic symmetry relaxes the constraints imposed on the domain walls geometry in EL by the orthorhombic symmetry, leading to a different variety of textures in the two phases. In all the 1D vector-wave phases, the twofold helical symmetry 2_1 cannot be broken, thus an additional order parameter is necessary for describing the helical structure of $B8$. For instance, an in-plane homogeneous polarization appearing at the Sm0 → $B8$ transition would break the equivalence of the two

TABLE V. Stable phases below EL ($B2$) when two waves, A and B, traveling along the same direction ($\vec{e}_x$ or $\vec{e}_y$), are condensed together.

Wave type	Phases A,B
$A+B$ $(\vec{K}=\vec{e}_x)$	AB_{Z^x}: $P2_1(z)$ C_2^2
$A+B$ $(\vec{K}=\vec{e}_x)$	AB^x: $P2(y)$ C_2^1
$A+B$ $(\vec{K}=\vec{e}_x)$	AB_{0^x}: $P1$ C_1^1
$A+B$ $(\vec{K}=\vec{e}_y)$	AB_{Z^y}: $P2_1(z)$ C_2^2
$A+B$ $(\vec{K}=\vec{e}_y)$	AB^y: $P2(x)$ C_2^1
$A+B$ $(\vec{K}=\vec{e}_y)$	AB_{0^y}: $P1$ C_1^1

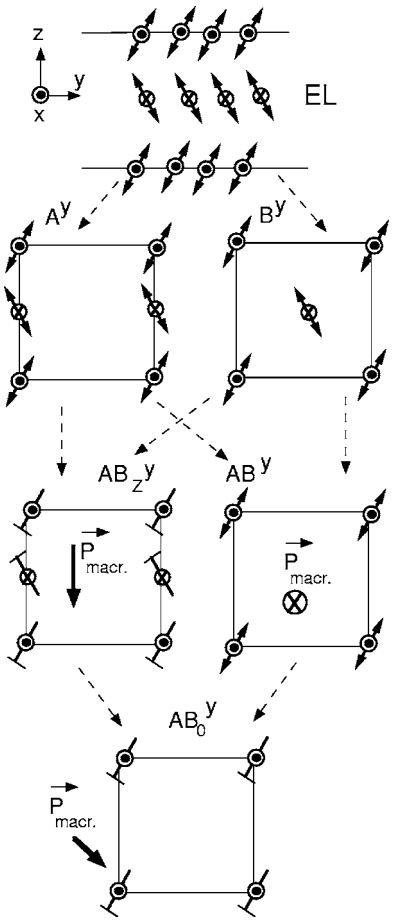

FIG. 8. AB-type subphases (Table V) of EL[$B2$], stabilized when the waves $A(\vec{e}_y)$ and $B(\vec{e}_y)$ condense simultaneously. The direction of the macroscopic polarization is indicated for the monoclinic AB^y, $AB_Z{}^y$, and triclinic $AB_O{}^y$ phases. In $AB_Z{}^y$ and $AB_O{}^y$ in-plane components of the molecular polarizations are omitted for clarity.

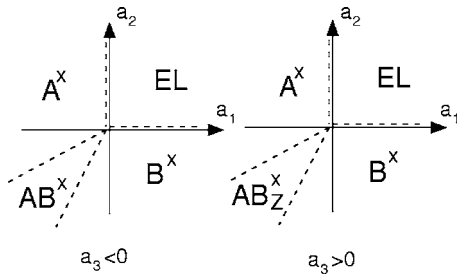

FIG. 9. Phase diagrams of the transition EL[$B2$] → $\{A^x, B^x\}$ → AB^x (or equivalently EL → $\{A^y, B^y\}$ → AB^y).

TABLE VI. List of the phases stabilized below the elliptic EL phase ($B2$) when $\vec{K}$ lies in the general direction of the x-y plane. The first row indicates the equilibrium conditions of the order-parameter components ψ_1 and ψ_2. The second row indicates the space groups and the dimensions of the stable phases.

$\psi_1=\psi_2=0$ (EL)	$\psi_2=0$ (I_E)	$\lvert\psi_1\rvert=\lvert\psi_2\rvert\neq 0$ (II_E)	$\lvert\psi_1\rvert\neq\lvert\psi_2\rvert$ (III_E)
$P222_1(z)$ D_2^2 (1D)	$P2_1(z)$ C_2^2 (2D)	$C222_1(z)$ D_2^2 (3D)	$P2_1(z)$ C_2^2 (3D)

layers related by 2_1 in EL′, yielding Bragg reflections at $q/2$ in the corresponding triclinic and ferrielectric B8 phase. Finally, the circular phase has not yet been directly observed, though several experimental observations led us [11] to propose that $B7$ is circular with a weak long-wavelength modulation along a direction normal to its helical axis. It is not the purpose of the present work to explain this modulation. On the other hand, the 2D and 3D structures of $B1$, $B3$, $B4$, $B5$, and $B6$ observed in bent-core systems [3] are not yet unambiguously clarified. The forthcoming analysis proposes a tentative identification of their structures and space groups.

The phases $B1$ and $B6$ exhibit close physical properties. B6 is stabilized on cooling under the isotropic liquid [3,22], with a layer spacing corresponding to one half of the molecular length. $B1$ has been observed either under the isotropic liquid or under $B6$ [22] in the sequence $I\rightarrow B6\rightarrow B1\rightarrow$Cry. Systems presenting simultaneously $B1$ and $B2$ are very rare (except when the $B1\rightarrow B2$ transition is induced under electric field [23]), making thus unlikely a group-subgroup relationship between their symmetries. No electro-optic switching is usually observed in $B6$, though such a behavior has been evidenced in media of asymmetric bent-core molecules with photoactive azo linkages [24]. $B1$ and $B6$ present similar fast dynamical molecular motions. The weakness of the high-frequency absorption in $B1$ supports an antiparallel alignment of the in-plane dipolar moments [22]. Finally, x-ray diffraction patterns in $B1$ show a rectangular 2D lattice.

The currently admitted structure model of $B1$ [3,25] coincides with the symmetry and the molecular configuration of the phase A_1^x pictured in Fig. 3(b). However, A_1^x is achiral whereas the achiral character of $B1$ is not systematically claimed in the literature [3]. The best chiral candidates are then A^x or A^y, because they have the closest chiral structure of A_1^x. A similar structural model has been proposed for explaining the fluctuating local molecular arrangement in the parent $B6$ phase [3,23], though it appears usually as an achiral smectic-type phase. We have to consider these observations with regard to the fact that in our approach the phase R is smectic and achiral, as well as its two primed analogs called $R\prime$ ($P2_1/m$) and $R\prime\prime$ ($Pmc2_1$) (obtained from R when the complex amplitudes of two linearly polarized waves [see Eq. (4)] with the same vector wave $\vec{k}$ have different phases [21]). Accordingly, we arrive provisionally at the following possible phase identifications: $B6$ is either R (R',R'') or A_1^x, whereas $B1$ corresponds either to A_1^x, A, or A^y, However, the symmetry refinement of $B1$ in Ref. [26] gives, using the 2D space-group notation, the group $P2mg$, i.e., in 3D notation, $Pma2$ (C_{2v}^4). This group being achiral, it rules out the hypothesis $B1=A^x$, A^y. On the other hand, $Pma2$, which is the space group of the phase $A_1^{y\prime}$, is polar so that, with this symmetry, $B1$ should be ferroelectric. Since no ferroelectricity is reported in this system [3,28], we guess the mirror symmetry parallel to the x-y plane has not been taken into account when $P2mg$ has been assigned to $B1$ (as it is always the case with the 2D notation). Since several 3D space groups can be "projected" onto a single 2D group, we assume that $P2mg$ represents in fact the apolar space group $Pmma$ [D_{2h}^5] of A_1^x instead of $Pma2$. The only remaining candidates for $B6$ are then the linear R phases (in Ref. [3], Pelzl *et al.* claim that the molecules are tilted in $B6$, yielding rather the identification with EL or EL′).

This identification ($B1=A_1^x$, $B6=R,R',R''$) is in agreement with the current interpretation describing $B6$ as an intercalated smectic structure with strong lateral fluctuations (see Fig. 11). Within this approach, $B6$ appears as a smectic proto-$B1$ phase, in which some molecules are intercalated between those located at the layers centers. Steric interactions exclude the covering of molecular arms so that, at the scale of a few molecules in $B6$, a fluctuating rectangular cell must appear when one molecule is intercalated. Let us notice that the corresponding local molecular configuration differs

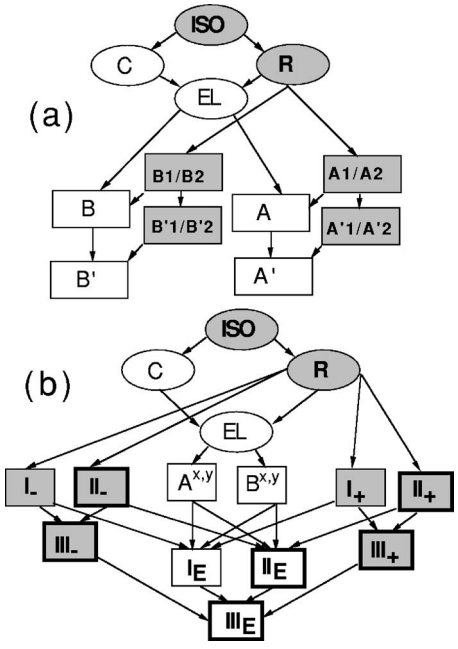

FIG. 10. Group-subgroup relationships. Elliptic, rectangular, and thick rectangular boxes indicate 1D, 2D, and 3D structures, respectively. The phases inside gray boxes are achiral. (a) When the wave vector is parallel to $\vec{e}_x$, the symbols A_i, B_i, A'_i, and B'_i, A and B represent A_1^x, A_2^x, etc. When the wave vector is parallel to $\vec{e}_y$, A_i, B_i, A'_i, and B'_i, A and B stand for the phases A_1^y, A_2^y, etc. (b) Phases induced from R (SmCP) or EL ($B2$) when the wave vector lies in the general direction of the smectic planes.

from that represented in Fig. 3 for A_1^x, where the interlayer spacing coincides with the molecular length. Since in this phase not even short-range translational order is observed in the plane normal to $\vec{k}$, the intercalated molecules must be randomly distributed. This suggests a disordering process for the $B1 \rightarrow B6$ transition, in which the phase θ of the polarization wave amplitude, $\psi = \rho e^{i\theta}$, becomes completely disordered, rather than a softening of the order parameter modulus ρ. Let us notice that, in this approach, the R phase, which is the parent structure of $B1$, has a lattice spacing equal to one molecular length L, whereas it is $2L$ in SmCP (R) and $B2$ (EL) (Fig. 11). This means that, although they belong formally to the same phase, SmCP and $B1$ arise from the isotropic phases with distinct order parameters: transverse polar waves with $k = \pi/L$ and $k = 2\pi/L$, respectively. Since SmCP and $B2$, on the one hand, and $B1$, on the other hand, appear almost never in the same phase diagram, it is not necessary to take into account these two waves simultaneously.

Several variants of $B1$ have been evidenced either in pure bent-core systems [27,28] or in mixtures [29]. In the columnar reversed $B1$ phase [28], denoted by $B1_{\mathrm{rev}}$, the space group is $Pmmn$ (which becomes $c2mm$ in the 2D notation, by suppressing the gliding mirror of $Pmmn$ parallel to $\vec{k}$ and $\vec{K}$), and the molecular polarizations are parallel to the columns. Its structure can be deduced from that of $B1$ after a fourfold clockwise rotation of all the molecules around $\vec{k}$ [23]. Its space group and its molecular structure coincide with the subphase B_1^y of R pictured in the first column of Fig. 4. A tilted variant of $B1_{\mathrm{rev}}$ has also been observed, called B_{X1} in Ref. [28]. Its chiral orthorhombic space group $P2_12_12$ (D_2^3) coincides with that of B^y in the configuration shown in Fig. 8. It can be reached from either $B2$ (EL) or SmCP (R) through second-order transition lines. From the analysis of x-ray patterns on well-developed monodomains, Pelzl *et al.* [26] proposed also the space groups $P11n$ (Pb, C_{1h}^2) and $Pm2_1n$ (C_{2v}^7) for another $B1$-type phase. The latter coincides with the symmetry of $B_1^{y\prime}$ (ferroelectric subphase of B_1^y), whereas the former can be only created by superposing a larger number of waves.

A three-dimensional phase labeled B_Y has been evidenced in compounds similar to those giving $B1$ and $B1_{\mathrm{rev}}$. Although its space group is not yet refined, Ref. [28] proposes a model structure that can be obtained by breaking the columns of $B1_{\mathrm{rev}}$ with a density wave parallel to the columns. Since the density wave does not break the point symmetry of $B1_{\mathrm{rev}}$, the corresponding space group is also $Pmmn$ (but with discrete translations along the three spatial directions). The authors of Ref. [28] claim, however, that an anticlinic ordering is more likely than a density wave. The simplest corresponding scenario, leading from the isotropic liquid to B_Y, involves at least three waves: (i) one polar transverse wave forming R, (ii) a second polar transverse wave [with the type $B_1(\vec{e}_y)$], with its wave vector normal to $\vec{k}$ and its polarization parallel to the polarization of the first wave, and (iii) an axial longitudinal axial wave [with the type $A_2(\vec{e}_x)$] with $\vec{A}$ parallel to the polarization. Then, the density wave breaking the columns turns out to be only a secondary (nonsymmetry-breaking) order parameter induced by the vector wave.

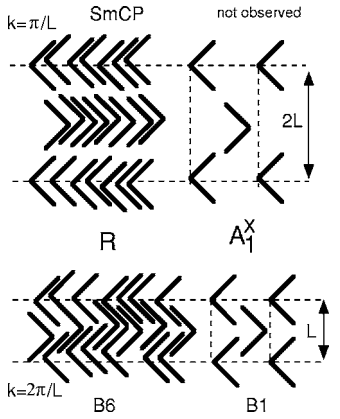

FIG. 11. Molecular structures of the phases R and A_1^x when $k = \pi/L$ (first row) and $k = 2\pi/L$ (second row). In the first row R represents the phase SmCP whereas the A_1^x structure has not been experimentally reported. In the second row, R represents the intercalated structure $B6$, and A_1^x the phase $B1$. The model by Roy *et al.* involves the nematic phase, SmCP (or $B2$), $B1$, and $B6$. The vector-wave theory relates the isotropic liquid (or the nematic) to SmCP and $B2$, on the one hand, and the isotropic phase (or nematic) to $B1$ and $B6$, on the other hand.

Hence, in terms of the wave types of the R space group, we denote conventionally this B_Y model by "$B_1(\vec{e}_y)+A_2(\vec{e}_x)$" (see Tables I and II). The unit-cell volume of the stable 3D phase is thus twice that obtained when the density wave is the symmetry-breaking order parameter. Its space group is the subgroup $Pccn$ (D_{2h}^{10}) of $Pmmn$. However, experimental results supporting this hypothesis are weak. Moreover, let us note that (i) the $B_1(\vec{e}_y)+A_2(\vec{e}_x)$ scenario is thermodynamically unlikely (because two nonequivalent symmetry-breaking representations of R must simultaneously condense), and (ii) neither R nor $B1_{\mathrm{rev}}$ have been reported in compounds where B_Y is observed, while such phases would be likely stabilized in the $B_1(\vec{e}_y)+A_2(\vec{e}_x)$ model. This leads us to propose an alternative interpretation where the phases $\mathrm{II}_\pm$ (which have the same point group D_{2h} as $Pccn$) are candidates for representing B_Y. The main advantage of this hypothesis is that it needs a single representation of R, and provides neither $B1$ nor $B1_{\mathrm{rev}}$ as stable phases.

Let us now discuss the lattice parameters measured in the various subphases of $B1$. In all cases, one unit cell contains a single molecule along Oz ($\vec{k}$), in agreement with the hypothesis of a parent R phase. In $B1$ the two cell parameters have similar magnitudes [3,30], which supports our initial assumption $|\vec{k}| \approx |\vec{K}|$. On the contrary, in $B1_{\mathrm{rev}}$ and B_Y the lattice parameters along $\vec{K}$ are much larger [28], so that one unit cell contains many molecules. This makes it less probable the direct transition from the isotropic liquid, but does not contradict the hypothesis of a common translational symmetry-breaking mechanism for the molecular ordering in the three directions. Indeed, the moduli of the corresponding wave vectors are influenced by short-range steric as well as by long-range electrostatic interactions. Thus, $|\vec{k}|$ should be very sensitive to the balance between the two interactions, and the corresponding length in the direction normal to Oz must depend on the preexisting molecular organization and may vary

significantly from one compound to one another. In the case when $|\vec{k}| \gg |\vec{K}|$ is observed, the vector-wave model starting from the isotropic phase with $|\vec{k}|=|\vec{K}|$ should be improved with a secondary (nonsymmetry-breaking) induced strain-tensor order parameter, which strongly expands the ordered unit cell in the x-y plane. Let us, however, note the following paradox: The equality $|\vec{k}| \approx |\vec{K}|$ comes from the hypothesis the waves along Oz, Ox, and Oy are, in the underlying isotropic state, of the same type (single mechanism). This equality is verified in $B1$, where the second wave is longitudinal instead of transverse, while it is violated for $B1_{\mathrm{rev}}$ where the two waves are transverse. This leads us to have doubts about the validity of the usual refinement of $B1$, and consequently about its identification with A_1^x.

The phases $B2$, $B3$, and $B5$ are characterized by their electro-optic switching [3,27]. In $B5$ [31], which appears on cooling $B2$ or $B6$ [32], density waves are observed in a direction perpendicular to $\vec{k}$, associated with a short-range 2D translational order. The corresponding unit cell is rectangular. Its electro-optic behavior is similar to that of $B2$ [20] and, presumably, both phases have the same point group. These properties of $B5$ are compatible with the phases A^x, A^y, B^x, and B^y (Table IV), which have a rectangular unit cell and the same orthorhombic (D_2) point group as EL (i.e., $B2$). They can be obtained either from C or EL through second-order transformations. On the other hand, Eremin *et al.* [33] have observed the following complex sequence $Iso \rightarrow B2 \rightarrow B'2 \rightarrow B''2 \rightarrow B5 \rightarrow B_X \rightarrow$ Cryst of transitions in a five-ring fluorinated bent-core mesogen. B_X denotes an orthogonal highly disordered 3D phase exhibiting electro-optic switching properties with a possible helical superstructure. $B'2$ and $B''2$ are also switchable and might be two-dimensional; however, their symmetries and structures are not given in Ref. [33]. Comparing the experimental sequence with the theoretical phase relations presented in Fig. 10(b) yields the following possibilities: $B_X=\mathrm{III_E}$, $B_5=\mathrm{I_E}$, and $B'2$, $B''2=A^x$, A^y, B^x, or B^y. They respect the group-subgroup relationships suggested by the observed transition sequence (except for $B2 \rightarrow B'2$), and they are in agreement with the chiral and dimensional features of the observed phases. However, the experimental data are too incomplete to rule out the possibilities $B_X=\mathrm{II_E}$ or $B5=A^x$, A^y, B^x, or B^y (but in this case the transition $B''2 \rightarrow B5$ would be reentrant).

$B3$ and $B4$ (often referred to as the "smectic blue" phase) appear on cooling after a sequence of phases involving $B2$. For instance, the sequence $Iso \rightarrow B2 \rightarrow B3 \rightarrow B4$ is reported by Jakli *et al.* [34] in pure achiral bent-core molecules and by Araoka *et al.* [35] in a mixture of chiral and achiral molecules. The shorter sequences, $Iso \rightarrow B2 \rightarrow B3 \rightarrow$ Cryst [36], $Iso \rightarrow B7 \rightarrow B4 \rightarrow$ Cryst [37], and $Iso \rightarrow B2 \rightarrow B4$ [38] can also be observed. Since $B3$ and $B4$ are chiral and three-dimensional, it follows that the single theoretical vector-wave candidates are $\mathrm{II_E}$ and $\mathrm{III_E}$. The monoclinic ferroelectric group of $\mathrm{II_E}$, being a subgroup of the $\mathrm{III_E}$ orthorhombic symmetry, it is natural to identify B3 with $\mathrm{III_E}$ and $B4$ with $\mathrm{II_E}$. Both being subphases of the chiral incommensurate modulated $B2$ phase, one expects helical modulations to occur in both structures if the crystalline order is weak enough. We have shown that $\mathrm{III_E}$ is nonpolar (point group D_2) while $\mathrm{II_E}$ is ferroelectric (point group C_2), property which is not observed in $B4$. Nevertheless, since the modulation could cancel the macroscopic polarization in $\mathrm{II_E}$, its identification with $B4$ remains possible.

Ferroelectricity is usually evidenced in liquid crystals either by the observation of a single peak in one half period of the current response to a triangular voltage, or by second harmonic generation experiments. Several smectic ($B2$ and $B7$) and columnar ($B5$) bent-core subphases exhibit sometimes this property [27,39]. These three phases have similar local structures and present either antiferroelectric or ferroelectric behaviors in various conditions. One can obtain such behaviors when, within our model, the complex amplitudes (e.g., ψ and ψ') of two copies of a single wave have different phases (e.g., $\theta \neq \theta'$). This happens, for instance, in the primed 1D helical C′ (point group C_∞) and elliptic EL′ (space group $P2_1$) phases [21], which may be thus associated with the observed ferroelectric variants of $B2$ and $B7$, respectively. The macroscopic polarization appears in these two cases in the direction of $\vec{k}$, making them antiferroelectric in the x-y plane and ferroelectric along Oz. The same mechanism can also lead to the ferrielectric phases $A'^{x,y}$, $B'^{x,y}$, which are thereby likely candidates for the polar $B5$ phase. Within this model ferroelectricity turns out to be a weak improper effect. Along this way, let us stress a major difference of our model with the popular heuristic interpretation in terms of homogeneous ordered layers packing [40]. In our approach, ferroelectricity is an induced secondary effect, resulting from the phase shift between primary antiferroelectric and anticlinic waves. On the contrary, in the layers packing approach, homogeneous polar layers are sticken either in ferroelectric (synclinic) or antiferroelectric (anticlinic) configurations, yielding at least four unlikely distinct primary mechanisms (density wave+homogeneous polar and axial vectors+vector waves). Moreover, in this case ferroelectricity would be a strong proper effect.

The previous analysis is summarized in Table VII. Crucial predictive features of the phenomenological approach concern the electric-field behaviors of the stable phases. Such behaviors can be theoretically studied for each separate phase, as we have done for the phases C, R, and EL in Ref. [11], and needs firstly a clear experimental identification of the corresponding zero-field molecular structures and wave patterns. As long as the observed structures are not definitely refined, theoretical identifications remain rather speculative. For instance, the models based on a TGB-type (twist-grain-boundary) state [35,41] or on a glassy state often claimed for $B4$, are sharply different from our identification with $\mathrm{II_E}$ and $\mathrm{III_E}$. Along this line we claim also the possibility of long-wavelength helical modulations in the elliptic and subelliptic phases [42]. However, we have not taken into account the possibility of a helical modulation for the vector wave itself, so that we are not able yet to predict or contradict the possibility of TGB behaviors in the vector-wave model.

B. Theories

Most of the available theories of bent-core systems deal with either nematic or smectic ($B2$, $B7$, SmCP) phases. Us-

ing a third-rank tensor order parameter Lubensky *et al.* [43] predict a number of low-symmetry nematics, which have not yet been evidenced but could be useful to understand the local molecular orientation in translationally ordered phases. They predict also a number of biaxial smectic phases, which are neither ferroelectric nor antiferroelectric and have thus no connection with the vector-wave phases. Along a different way, we have used two second-rank tensors [44] to describe the possible orientation orders arising in the uniaxial and biaxial phases observed with bent-core molecules. Vanakaras *et al.* [45] predict uniaxial and biaxial nematic and smectic phases in liquids of biaxial molecules. Kats *et al.* [46] study the transitions between Sm*A* and *B*2 with an order parameter consisting of axial and polar vectors together with a pseudoscalar. This approach is similar to the vector-wave approach when one only considers the *B*2 phase. Analogously, Selinger [47] uses a pseudoscalar wave condensing in the smectic *A* phase in which the polar order preexists. He explains thus the chiral symmetry breaking in *B*2 but not its vector character. Roy *et al.* [48] start also from the Sm*A* phase, in the layers of which axial and polar coupled vectors yield tilt and polarization orders characteristic of bent-core smectic phases. It is usually claimed in the literature that *B*2 can appear with four different structures, denoted by $\mathrm{Sm}C_{\mathrm{S,F}}P_{\mathrm{A,F}}$ according to the synclinic/anticlinic and ferroelectric/antiferroelectric possible interlayer configurations. This point of view is contradictory with our phenomenological approach. Indeed, it assumes the condensation of several nonequivalent order parameters in Sm*A*: axial and polar waves together with axial and polar homogeneous vectors. This implies the very unlikely simultaneous condensation of five distinct order parameters (including the Sm*A* density wave) in the isotropic liquid. Moreover, the various stable phases should be then very different since they are related to completely distinct (at the symmetry point of view) ordering mechanisms. For us, the single possibility for *B*2 is $\mathrm{Sm}C_{\mathrm{A}}P_{\mathrm{A}}$ (i.e., EL) whereas the antiferroelectric variant of *R* can be represented by $\mathrm{Sm}AP_{\mathrm{A}}$ (or $\mathrm{Sm}AC_{\mathrm{A}}$ for its anticlinic variant), which both arise from a single mechanism in the isotropic liquid (or possibly from the nematic or Sm*A* phases).

On the other hand, only very few theoretical works have yet been devoted to the 2D and 3D bent-core phases. Vaupotic *et al.* [49] propose a model describing in-plane modulations in *B*2 giving rise to the modulated *B*7 phase (that we have considered as approximately 1D at the beginning of this section). In Ref. [49], the parent *B*2 phase is assumed to be in the $\mathrm{Sm}C_{\mathrm{S}}P_{\mathrm{F}}$ configuration, i.e., with a synclinic and ferroelectric order. Although this configuration is not permitted by our approach, in which all the 1D phases are anticlinic and antiferroelectric, the idea involving a long-wavelength modulation of the *B*2 structure is similar to our own point of view concerning *B*7. To our knowledge, there exists a single theoretical work, by Roy *et al.* [50], accounting for the columnar bent-core phases. These authors remarked that, although *B*1/*B*6 and *B*2 are seldom stabilized in a single compound, the sequence $B6 \rightarrow B1 \rightarrow B2$ is often observed by increasing the chain length of the molecules. A theoretical study of this sequence compels to take into account the difference in the lattice spacings 2L and *L* of *B*2 and *B*1 (or *B*6) [see Fig. 11]. In this goal, they introduce

TABLE VII. Identification of the bent-core states with the phases stabilized in the vector-wave model.

Phases	Nonferroelectric	Ferroelectric
Sm*CP*	*R*	
*B*1	A_1^x	
$B1_{\mathrm{rev}}$	B_1^y	$B_1^{y\prime}$
B_Y	$B_1(\vec{e}_y)+A_2(\vec{e}_x)$, $\mathrm{II}_{\pm}$	
B_{X1}	$B^{x,y}$	
*B*2	EL	C′, EL′
B′2	$A^{x,y}$, $B^{x,y}$	
B″2	$A^{x,y}$, $B^{x,y}$	
*B*3	$\mathrm{III}_{\mathrm{E}}$	
*B*4	II_{E}	
*B*5	$A^{x,y}$, $B^{x,y}$	$A'^{x,y}$, $B'^{x,y}$
B_X	II_{E}, $\mathrm{III}_{\mathrm{E}}$	
*B*6	*R*, *R*′, *R*″	
*B*7	C	C′, EL′
Sm0		EL′
*B*8		

three density waves in the uniaxial nematic phase, with wave vectors $k_0\vec{e}_z+k_x\vec{e}_x$, $k_0\vec{e}_z-k_x\vec{e}_x$, and $2k_0\vec{e}_z$, where $k_0=\pi/L$ (*L* is the molecular length) coupled with a transverse vector wave P_A. When $k_x=0$, the *B*2 phase (in fact, it is rather the Sm*CP* phase, i.e. *R*, since they neglect the molecular tilt) is stabilized. When the density waves $k_0\vec{e}_z\pm k_x\,\vec{e}_x$ vanish, *B*6 is stabilized whereas *B*1 appears when the three order parameters onset simultaneously. The nematic $\rightarrow B6$ transition is predicted to be second order whereas all the other transitions are first order. Let us remark that the wave vector of the polarization wave P_A is not fixed in the model by Roy *et al.* since it is equal to $k_0\vec{e}_z$ in Sm*CP* and to $2k_0\vec{e}_z$ in *B*6, so that in fact two such waves should be incorporated in their model. With this additional vector wave $(2k_0\vec{e}_z)$ the third density wave $(2k_0\vec{e}_z)$ turns out to be, as in the vector-wave model, a secondary order parameter without significant physical effects.

This model has various common features with the vector-wave approach because it involves polar and scalar waves [in our theory the wave $A_1(\vec{e}_x)$ might also be a density wave]. However, the set of waves used by Roy *et al.* is slightly different from that in our theory. In particular, in our approach the density waves are normal to *Oz*: $\vec{k}=\pm k_x\vec{e}_x$ whereas they are not in Ref. [50]. On the other hand, their model [50] is "richer" because it involves simultaneously waves with wave vectors $k_0\vec{e}_z$ (when $k_x=0$) and $2k_0\vec{e}_z$. Thus, the vector-wave model works out separately the transitions nematic $\rightarrow$ Sm*CP* (*R*) $\rightarrow B2$ (EL) and nematic $\rightarrow B6$ (*R*) $\rightarrow B1$ (A_1^x), while Ref. [50] works out simultaneously the transitions nematic $\rightarrow$ Sm*CP* $\rightarrow B \rightarrow B1$ (in the vector-wave model, the parent phase may be nematic as well as isotropic).

(i) Focusing attention on the $B6 \rightarrow B1$ transition reveals the following difference: In our theory this transition is spanned by a two-branch longitudinal polar (or density) wave, while it is spanned by a four-branch density wave in Ref. [50]. This yields second- and first-order transitions at

the lowest degree approximation of the free energy, in the vector wave and the density wave approaches, respectively.

(ii) Finally, let us notice that in Ref. [50], the nematic $\rightarrow$ SmCP transition results from the condensation of the vector wave P_A and of the density wave $\vec{k}=2k_0\vec{e}_z$. However, the density wave is in this case a secondary (nonsymmetry-breaking) order parameter, induced by the primary condensation of P_A. This description coincides thus exactly with that of the vector-wave model.

The vector-wave approach provides a unified and physically coherent scheme including a large class of bent-core mesophases. Our work shows that a single mechanism might explain the complex polymorphism observed in this family of materials. Indeed, the phases made with such molecules present strong physical similarities and are often distinguished only by tenuous effects, whereas they are immediately distinguished from other known liquid crystals. These features support the idea of a common mechanism underlying the stabilization of most translationally ordered bent-core mesophases. The hypothesis of a single transverse-wave condensation accounting for the uni-, bi-, and tri-dimensional bent-core phases is not yet completely satisfactory since the commonly accepted structure of $B1$ results from the condensation of a longitudinal wave in R. Nevertheless, $B1$ is perfectly characterized as a subphase of R, which itself results from the condensation of a transverse wave in the isotropic liquid. On the other hand, we have seen that 15 among the 23 phases (included 1D) resulting from a transverse wave are fair candidates for the identification of the other bent-core phases or subphases. Conversely, all the observed phases, except (maybe) $B1$, are compatible with the transverse vector-wave mechanism. This provisional success of the vector-wave model in the class of columnar and soft-crystalline phases supports the general validity of this approach in the whole field of bent-core phases.

ACKNOWLEDGMENT

I acknowledge helpful discussions with V. Lorman.

APPENDIX

The symmetry-breaking mechanisms presented in Secs. III and IV are classified according to irreducible representations of the high-symmetry space groups of R ($Pmma$), C ($\infty_1 22$), and EL ($P222_1$). These representations are completely characterized by their wave vectors $\vec{K}$ and by the small representations of the corresponding $\vec{K}$ point groups. Unlike $\vec{k}^*$ in the isotropic liquid, the little groups are discrete and $\vec{K}^*$ possesses a finite number of branches (except in C). We consider only the representations with wave vectors $\vec{K}$ normal to $\vec{k}$. Since the Brillouin zones of R, C, and EL are unbounded (1D phases are homogeneous in the x-y plane), the irreducible representations are direct products of one tensor (irreducible representation of the little group [13]) with n scalar sinusoidal waves, where n is the number of branches in $\vec{K}^*$.

1. In R

In R, three nonequivalent directions in the reciprocal x-y plane (normal to $\vec{k}$) give distinct little groups, as follows:

(1) $\vec{K}=\mathrm{K}_x\vec{e}_x$. The star $\vec{K}^*$ of $\vec{K}$ has two branches. The little group (C_{2v}) has four nonequivalent one-dimensional small representations, denoted by A_1, A_2, B_1, and B_2 (see Ref. [13]). They transform respectively as a scalar, an axial vector parallel to Oz, a polar vector parallel to Ox, and a polar vector parallel to Oy. They yield four two-dimensional irreducible representations of $Pmma$, which we denote by $A_1(\vec{e}_x)$, $A_2(\vec{e}_x)$, $B_1(\vec{e}_x)$, and $B_2(\vec{e}_x)$. The symmetries of the general directions in each of these spaces are larger than the kernels of the corresponding representations. Thus, the mechanism associated with these representations must be completed by enlarging the representation spaces. This completion leads to the following reducible representations of $Pmma$: $A_1(\vec{e}_x)\oplus A_1(\vec{e}_x)$, $A_2(\vec{e}_x)\oplus A_2(\vec{e}_x)$, $B_1(\vec{e}_x)\oplus B_1(\vec{e}_x)$, and $B_2(\vec{e}_x)\oplus B_2(\vec{e}_x)$. For each of them, the general direction has the same symmetry group as the kernel, corresponding to the so-called primed phases.

(2) $\vec{K}=K_y$. $\vec{K}^*$ has two branches. The little group is again C_{2v}, with the same four small representations A_1, A_2, B_1, and B_2. They transform respectively as a scalar, an axial vector parallel to Oz, a polar vector parallel to Oy, and a polar vector parallel to Ox. The corresponding irreducible representations $A_1(\vec{e}_y)$, $A_2(\vec{e}_y)$, $B_1(\vec{e}_y)$, and $B_2(\vec{e}_y)$ are two-dimensional and yield nonminimal groups. The complete reducible representations associated with these mechanisms are, thus, $A_1(\vec{e}_y)\oplus A_1(\vec{e}_y)$, $A_2(\vec{e}_y)\oplus A_2(\vec{e}_y)$, $B_1(\vec{e}_y)\oplus B_1(\vec{e}_y)$, and $B_2(\vec{e}_y)\oplus B_2(\vec{e}_y)$.

(3) $\vec{K}=K_x\vec{e}_x+K_y\vec{e}_y$. Its star contains four branches. The little group C_S is generated by the mirror plane normal to Oz and has two one-component small representations denoted by R_+ and R_-. They transform as a scalar and a vector parallel to Oz, respectively. The corresponding irreducible four-dimensional representations of $Pmma$ are $R_+(\vec{K})$ (e.g., four scalar waves) and $R_-(\vec{K})$ (e.g., four transverse vector waves). The corresponding general directions have the same symmetry as the kernel so that these irreducible representations yield complete mechanisms.

2. In C

In C, $\vec{K}^*$ has infinitely many branches forming a circle in the reciprocal space. A and B denote the two small representations associated with the little group C_2 of $\vec{K}$. They transform respectively as a scalar and a vector normal to $\vec{K}$. $A(\vec{K})$ and $B(\vec{K})$ have an infinite number of components spanned by scalar waves or transverse (axial or polar) vector waves, respectively, traveling in all the directions of the x-y plane.

We consider only the simplest case in which two branches, $\vec{K}$ and $-\vec{K}$, become active at the transition. The choice of the direction of $\vec{K}$ is arbitrary since the symmetry group of C ($\infty_1 22$) is isotropic in the x-y plane. Changing this direction (i.e., varying the corresponding Goldstone angle) amounts to generate other equivalent domains of the same

ordered phases. $A(\vec{K})$ and $B(\vec{K})$ become then finite dimensional since they both are spanned by only two waves. They span irreducible representations of the space group $T \times C_2$, where T is the translation group of C. Likewise in R, two isomorphic copies of such irreducible representations are necessary to stabilize all the accessible low-symmetry structures, so that the most general 16-dimensional representation is $A(\vec{K}) \oplus A(\vec{K}) \oplus B(\vec{K}) \oplus B(\vec{K})$. The stable ordered phases are then the same as the subphases of EL.

3. In EL

The space group of EL is a subgroup of both R and C groups. The irreducible representations of C and R become reducible in EL. In addition, nonequivalent representations in C and R may become equivalent in EL. Comparing with R is more easy. Again one has to consider three directions for $\vec{K}$.

(1) $\vec{K}=K_x\vec{e}_x$, $\vec{K}^*$ has two branches. The little group is C_2 instead of C_{2v} in R. The small representations A_1 and A_2 of C_{2v} become equivalent in C_2 and give rise to the single small representation denoted by A, whereas B_1 and B_2 give rise to B. They transform respectively as a scalar and a polar vector parallel to Ox. The two-dimensional irreducible representations $A(\vec{e}_x)$ and $B(\vec{e}_x)$ are spanned by two scalar waves and two transverse polar vector waves, respectively. As in R, two copies of these representations are necessary to complete the corresponding symmetry-breaking mechanisms, which are thus associated with the reducible representations $A(\vec{e}_x) \oplus A(\vec{e}_x)$ and $B(\vec{e}_x) \oplus B(\vec{e}_x)$.

(2) $\vec{K}=K_y\vec{e}_y$. $\vec{K}^*$ has two branches. The little group is C_2 instead of C_{2v} in R. The same collapse of the R irreducible representations yields two irreducible mechanisms: $A(\vec{e}_y)$ and $B(\vec{e}_y)$ spanned by two scalar waves and two transverse vector waves. The complete mechanism correspond to the reducible four-dimensional representations $A(\vec{e}_y) \oplus A(\vec{e}_y)$ and $B(\vec{e}_y) \oplus B(\vec{e}_y)$.

(3) $\vec{K}=K_x\vec{e}_x+K_y\vec{e}_y$. Its star contains four branches. The little group is reduced to the identity and has a single scalar representation. The corresponding irreducible four-dimensional representation of *Pmma* is spanned, for instance, by a set of four scalar waves.

[1] R. B. Meyer, L. Liebert, L. Strzelecki, and P. Keller,J. Phys. (Paris), Lett. **36**, L69 (1975).

[2] T. Niori, T. Sekine, J. Watanabe, T. Furukawa, and H. Takezoe, J. Mater. Chem. **6**, 1231 (1996).

[3] G. Pelzl, S. Diele, and W. Weissflog, Adv. Mater. (Weinheim, Ger.) **11**, 707 (1999).

[4] R. Macdonald, F. Kentischer, P. Warnick, and G. Heppke, Phys. Rev. Lett. **81**, 4408 (1998).

[5] D. R. Link, G. Natale, R. Shao, J. E. Maclennan, N. A. Clark, E. Korblova, and D. M. Walba, Science **278**, 1924 (1997).

[6] A. Eremin, S. Diele, G. Pelzl, H. Nadasi, W. Weissflog, J. Salfetnikova, and H. Kresse, Phys. Rev. E **64**, 051707 (2001).

[7] G. Pelzl, S. Diele, A. Jakli, Ch. Lischka, I. Wirth, and W. Weissflog, Liq. Cryst. **26**, 135 (1999).

[8] T. Sekine, T. Niori, M. Sone, J. Watanabe, S. W. Choi, Y. Takanishi, and H. Takezoe, Jpn. J. Appl. Phys., Part 1 **36**, 6455 (1999).

[9] T. Sekine, Y. Takanishi, T. Niori, J. Watanabe, and H. Takezoe, Jpn. J. Appl. Phys., Part 2 **36**, L1201 (1997).

[10] L. D. Landau, *Collected Papers* (Pergamon, New York, 1965), p. 21; S. Alexander and J. McTague, Phys. Rev. Lett. **41**, 702 (1978).

[11] V. Lorman and B. Mettout, Phys. Rev. Lett. **82**, 940 (1999); V. Lorman and B. Mettout, Phys. Rev. E **69**, 061710 (2004).

[12] J. C. Tolédano and P. Tolédano, *The Landau Theory of Phase Transitions* (World Scientific, Singapore, 1987).

[13] C. J. Bradley and A. P. Cracknell, *The Mathematical Theory of Symmetry in Solids*, (Clarendon Press, Oxford, 1972). We use the notation of this reference for the small representations $A1$, $A2$, $B1$, and $B2$ of C_{2v} (p. 58), whereas we use the notations $R_\pm$ for the small representations of the point groups C_S.

[14] L. D. Landau, Zh. Eksp. Teor. Fiz. **7**, 627 (1937).

[15] V. L. Idenbom, S. A. Pikin, and E. B. Loginov, Sov. Phys. Crystallogr. **21**, 632 (1976); S. A. Pikin and V. L. Idenbom, Sov. Phys. Usp. **21**, 487 (1978); V. L. Idenbom and E. B. Loginov, Sov. Phys. Crystallogr. **26**, 526 (1981).

[16] P. G. de Gennes and J. Prost, *The Physics of Liquid Crystals* (Oxford University Press, Oxford, 1993).

[17] Yu. M. Gufan, *Structural Phase Transitions* (Nauka, Moscow, 1982).

[18] B. Mettout and P. Tolédano, Europhys. Lett. **46**, 357 (1999).

[19] B. Mettout, P. Tolédano, and V. Lorman, Phys. Rev. Lett. **77**, 2284 (1996).

[20] J. P. Bedel, J. C. Rouillon, J. P. Marcerou, M. Laguerre, H. T. Nguyen, and M. F. Achard, Liq. Cryst. **28**, 1285 (2001).

[21] B. Mettout and V. Lorman (unpublished).

[22] H. Kress, H. Schmalfuss, and W. Weissflog, Liq. Cryst. **28**, 799 (2001); W. Weissflog, F. Wirth, S. Diele, G. Pelzl, H. Schmalfuss, T. Schoss, and A. Würflinger, *ibid.* **28**, 1603 (2001).

[23] J. Ortega, M. R. de la Fuente, J. Etxebarria, C. L. Folcia, S. Dıez, J. A. Gallastegui, N. Gimeno, M. B. Ros, and M. A. Pérez-Jubindo, Phys. Rev. E **69**, 011703 (2004).

[24] V. Prasad, D. S. Shankar Rao, and S. Krishna Prasad, Liq. Cryst. **28**, 643 (2001).

[25] J. Watanabe, T. Niori, T. Sekine, and H. Takezoe, Jpn. J. Appl. Phys., Part 2 **37**, L139 (1998).

[26] D. Shen, S. Diele, G. Pelzl, I. Wirth, and C. Tschierske, J. Mater. Chem. **9**, 661 (1999); K. Pelzl, W. Weissflog, U. Baumeister, and S. Diele, Liq. Cryst. **30**, 1151 (2003).

[27] C. Tschierske and G. Dantlgraber, Pramana, J. Phys. **61**, 455 (2003).

[28] J. Szydlowska, J. Mieczkowski, J. Matraszek, D. W. Bruce, E. Gorecka, D. Pociecha, and D. Guillon, Phys. Rev. E **67**, 031702 (2003).

[29] R. Pratibha, N. V. Madhusudana, and B. K. Sadashiva, Phys.

Rev. E **71**, 011701 (2005).
[30] R. Amaranatha Reddy and B. K. Sadashiva, Liq. Cryst. **30**, 1031 (2003).
[31] S. Diele, S. Grande, H. Kruth, C. Lischka, G. Pelzl, W. Weissflog, and I. Wirth, Ferroelectrics **212**, 169 (1998).
[32] E. Matuys and K. Fodor-Csorba, Liq. Cryst. **30**, 445 (2003).
[33] A. Eremin, I. Wirth, S. Diele, G. Pelzl, H. Schmalfuss, H. Kresse, H. Nadasi, K. Fodor-Csorba, E. Gacs-Baitz, and W. Weissflog, Liq. Cryst. **29**, 775 (2002).
[34] A. Jakli, S. Rauch, D. Lötzsch, and G. Heppke, Phys. Rev. E **57**, 6737 (1998).
[35] F. Araoka, N. Y. Ha, Y. Kinoshita, B. Park, J. W. Wu, and H. Takezoe, Phys. Rev. Lett. **94**, 137801 (2005).
[36] G. Heppke, A. Jakli, and S. Rauch, Phys. Rev. E **60**, 5575 (1999); H. Kresse, J. Salfetnikova, H. Nadasi, W. Weissflog, and A. Hauser, Liq. Cryst. **28**, 1017 (2001).
[37] V. Prasad, Liq. Cryst. **28**, 1115 (2001).
[38] J. Ortega, N. Pereda, C. L. Folcia, J. Etxebarria, and B. Ros, Phys. Rev. E **63**, 011702 (2000).
[39] J. P. Bedel, J. C. Rouillon, J. P. Marcerou, M. Laguerre, H. T. Nguyen, and M. F. Achard, Liq. Cryst. **27**, 1411 (2000); H. Nadasi, W. Weissflog, A. Eremin, G. Pelzl, S. Diele, B. Das, and S. Grande, J. Mater. Chem. **12**, 1316 (2002); R. Amaranatha Reddy and B. K. Sadashiva, *ibid.* **12**, 2627 (2002); F. Araoka, H. Hoshi, and H. Takezoe, Phys. Rev. E **69**, 051704 (2004); E. Gorecka, D. Pociecha, F. Araoka, D. R. Link, M. Nakata, J. Thisayukta, Y. Takanishi, K. Ishikawa, J. Watanabe, and H. Takezoe, *ibid.* **62**, R4524 (2000).
[40] H. R. Brand, P. E. Cladis, and H. Pleiner, Eur. Phys. J. B **B6**, 347 (1998); D. M. Walba, E. Korblova, R. Shao, J. E. Maclennan, D. R. Link, M. A. Glaser, and N. A. Clark, Science **288**, 2181 (2000).
[41] T. Sekine, T. Niori, M. Sone, J. Watanabe, S. W. Choi, Y. Takanishi, and H. Takezoe, Jpn. J. Appl. Phys., Part 1 **36**, 6455 (1997); P. Collings, G. Heppke, D. Kruerke, C. Lohnig, J. Rabe, and W. Stocker, in *Abstracts of the Workshop on Banana-Shaped Liquid Crystals* edited by G. Heppke (Technical University of Berlin, Berlin, 1997).
[42] F. Kentischer, R. Macdonald, P. Warnick, and G. Heppke, Liq. Cryst. **25**, 341 (1998).
[43] T. C. Lubensky, and Leo Radzihovsky, Phys. Rev. E **66**, 031704 (2002).
[44] B. Mettout, Phys. Rev. E **72**, 031706 (2005).
[45] A. G. Vankaras, M. A. Bates, and D. J. Photinos, Phys. Chem. Chem. Phys. **5**, 3700 (2003).
[46] E. I. Kats and J. Lajzerowicz, e-print cond-mat/9912486.
[47] J. V. Selinger, Phys. Rev. Lett. **90**, 165501 (2003).
[48] A. Roy, N. V. Madhusudana, P. Tolèdano, and A. M. Figueiredo Neto, Phys. Rev. Lett. **82**, 1466 (1999).
[49] N. Vaupotic and M. Copic, Phys. Rev. E **72**, 031701 (2005).
[50] A. Roy and N. V. Madhusudana, Eur. Phys. J. E **18**, 253 (2005).